KTH Industrial Engineering
and Management

Enhanced Boiling Heat Transfer on a Dendritic and Micro-Porous Copper Structure

Doctoral Thesis by Richard Furberg

Stockholm, November 2011

KTH School of Industrial Engineering and Management
Department of Energy Technology
Division of Applied Thermodynamics and Refrigeration

KTH Industrial Engineering
and Management

Enhanced Boiling Heat Transfer on a Dendritic and Micro-Porous Copper Structure

Doctoral Thesis by Richard Furberg

Stockholm, November 2011

KTH School of Industrial Engineering and Management
Department of Energy Technology
Division of Applied Thermodynamics and Refrigeration

TRITA REFR Report No 11/02
ISSN 1102-0245
ISRN KTH/REFR/11/02-SE
ISBN 978-91-7501-163-9

Abstract

A novel surface structure comprising dendritically ordered nano-particles of copper was developed during the duration of this thesis research project. A high current density electrodeposition process, where hydrogen bubbles functioned as a dynamic mask for the materials deposition, was used as a basic fabrication method. A post processing annealing treatment was further developed to stabilize and enhance the mechanical stability of the structure.

The structure was studied quite extensively in various pool boiling experiments in refrigerants; R134a and FC-72. Different parameters were investigated, such as; thickness of the porous layer, presence of vapor escape channels, annealed or non-annealed structure. Some of the tests were filmed with a high speed camera, from which visual observation were made as well as quantitative bubble data extracted. The overall heat transfer coefficient in R134a was enhanced by about an order of magnitude compared to a plain reference surface and bubble image data suggests that both single- and two-phase heat transfer mechanisms were important to the enhancement.

A quantitative and semi-empirical boiling model was presented where the main two-phase heat transfer mechanism inside the porous structure was assumed to be; micro-layer evaporation formed by an oscillating vapor-liquid meniscus front with low resistance vapor transport through escape channels. Laminar liquid motion induced by the oscillating vapor front was suggested as the primary single-phase heat transfer mechanism.

The structure was applied to a standard plate heat exchanger evaporator with varying hydraulic diameter in the refrigerant channel. Again, a 10 times improved heat transfer coefficient in the refrigerant channel was recorded, resulting in an improvement of the overall heat transfer coefficient with over 100%. A superposition model was used to evaluate the results and it was found that for the enhanced boiling structure, variations of the hydraulic diameter caused a change in the nucleate boiling mechanism, which accounted for the largest effect on the heat transfer performance. For the standard heat exchanger, it was mostly the convective boiling mechanism that was affected by the change in hydraulic diameter.

The structure was also applied to the evaporator surface in a two-phase thermosyphon with R134a as working fluid. The nucleate boiling mechanism was found to be enhanced with about 4 times and high speed videos of the enhanced evaporator reveal an isolated bubble flow regime, similar to that of smooth channels with larger hydraulic diameters. The number and frequency of the produced bubbles were significantly higher for the enhanced surface compared to that of the plain evaporator. This enhanced turbulence and continuous boiling on the porous structure resulted in decreased oscillations in the thermosyphon for the entire range of heat fluxes.

Keywords: enhanced boiling; R134a; FC-72; flow boiling; heat transfer; high speed visualization; instability; micro-channels; micro-structured; nano- and micro-technology; nano- and micro-porous structured surfaces; plate heat exchanger; pool boiling; porous media; thermosyphon; two-phase heat transfer

Sammanfattning

En ny ytstruktur, bestående av dendritiskt ordnade nanopartiklar av koppar, har utvecklats inom ramen för detta doktorandprojekt. Den grundläggande tillverkningsmetoden var elektrodeposition med hög strömdensitet där vätgasbubblor formade en dynamisk mall under depositionen. En värmebehandling utvecklades där strukturen stabiliserades och dess mekaniska egenskaper förbättrades.

Ytstrukturen studerades ingående under olika kärlkokningsexperiment i medierna R134a och FC-72. Olika parametrar studerades, så som; ytstrukturens tjocklek, betydelsen av gasutsläppskanaler, inverkan av värmebehandling samt olika medier. Somliga tester filmades med en höghastighetskamera vars bilder analyserades både kvalitativt och kvantitativt. Värmeövergångstalet i R134a förbättrades med en faktor tio jämfört med en referensyta i koppar och bubbeldata antyder att värmeövergångsmekanismerna vid både en- och tvåfas var viktiga för förbättringen.

En kvantitativ och delvis empirisk kokningsmodell utvecklades. Den huvudsakliga värmetransportmekanismen vid tvåfas övergång föreslogs vara förångning av tunna ytskikt som formats av en oscillerande gasfront och där gasen transporteras med lågt friktionsmotstånd genom gasutsläppskanaler. Laminärt vätskeflöde som inducerats av den oscillerande gasfronten föreslogs vara den primära enfasmekanismen för värmetransporten.

Ytstrukturen applicerades på en vanlig plattvärmeväxlare med olika hydrauliska diametrar i köldmediekanalen. En tiofaldig ökning av värmeövergångstalet på köldmediesidan uppmättes, vilket motsvarade en fördubbling av värmeväxlarens UA-värde. En additiv modell användes för att utvärdera resultaten vilken pekade på att olika hydrauliska diametrar ledde till en förändring av den dominerande tvåfasmekanismen för den porösa ytan. För den obehandlade värmeväxlaren påverkades å andra sidan den konvektiva enfasmekanismen av variationer i den hydrauliska diametern.

Strukturen tillämpades också på förångaren till en tvåfas termosifon med R134a som arbetsmedium. Kärlkokningsmekanismen förbättrades ungefär fyra gånger och bilder från höghastighetskameran visade på en flödesregim med isolerade bubblor, liknande den för släta förångare med större hydrauliska diametrar. Bubbelfrekvensen var betydligt högre för förångaren med ytstrukturen jämfört med den släta förångaren. Därmed förbättrades turbulensen och den stadigvarande kokningen i ytstrukturen vilka ledde till mindre amplitud i egensvängningarna i termosifonen över hela det testade området av värmeeffekter.

Nyckelord: förbättrad kokning; R134a; FC-72; flödeskokning; värmetransport; höghastighetsfilmning; instabilitet; mikrokanaler; nanoteknologi; nano- och mikroporösa ytstrukturer; plattvärmeväxlare; kärlkokning; poröst media; termosifon; tvåfas värmetransport

Acknowledgments

First of all, many thanks to my supervisor Prof. Björn Palm, for his invaluable support, help, insight and guidance. I would also like to express my gratitude to Prof. Mamoun Muhammed, Muhammet Toprak, and Shanghua Li for being willing and able to make this work progress and develop in an exciting direction.

Plenty of Mahalo also goes out to all you helpful colleagues at the department of Applied Thermodynamics and Refrigeration who have assisted me with everything from practical help to insightful advice on how to make progress in my research.

Finally, I am incredibly thankful for and to my wife for their innumerable encouragements when experiments were failing and the work seemed to advance too slowly. Thanks for helping me to constantly refocus on what is really important in life.

Publications

Most of this thesis is based on the following publications. The journal and conference publications are attached in appendix I-VI.

Licenciate Thesis

Furberg, R., 2006, *Enhanced Boiling Heat Transfer From a Novel Nanodendritic Micro-Porous Copper Structure*, ISSN 1102-0245, Licentiate thesis at Royal Institute of Technology, Stockholm, Sweden

Pool Boiling Experiments of the Nanostructured Macro-porous Structure

I. Richard Furberg, Shanghua Li, Björn Palm, Muhammet Toprak, Mamoun Muhammed, 2006, *Dendritically Ordered Nano-Particles in a Micro-Porous Structure for Enhanced Boiling*, Proceedings of IHTC-13 conference, Sydney, AU.

II. Shanghua Li, Richard Furberg, Muhammet Toprak, Björn Palm, Mamoun Muhammed, 2008, *Nature-inspired Boiling Enhancement by Novel Nanostructured Macro-porous Surface*, Advanced Functional Material, Vol. 18, pp. 2215–2220.

III. Richard Furberg and Björn Palm, 2011, *Boiling Heat Transfer on a Dendritic and Microporous Surface in R134a and FC-72*, Applied Thermal Engineering, 31, pp. 3595-3603.

Application of the enhancement structure in a plate heat exchanger

IV. Richard Furberg, Björn Palm, Shanghua Li, Muhammet Toprak, Mamoun Muhammed, 2009, *The Use of a Novel Nano- And Micro-Porous Structure For Enhanced Boiling In a Plate Heat Exchanger*, Journal of Heat Transfer (special edition on porous media heat transfer), Vol. 131 (10).

Application of the enhancement structure in a thermosyphon

V. Richard Furberg, Rahmatollah Khodabandeh, Björn Palm, Shanghua Li, Muhammet Toprak, Mamoun Muhammed, 2008, *Experimental Investigation of an Evaporator Enhanced With a Micro-Porous Structure in a Two-Phase Thermosyphon Loop*, Proceedings of 2008 ASME Summer Heat Transfer Conference, HT2008, August 10-14, Jacksonville, Florida USA.

VI. Rahmatollah Khodabandeh, Richard Furberg, 2010, *Heat Transfer, Flow Regime and Instability of a Nano- and Micro-Porous Structure Evaporator in a Two-Phase Thermosyphon Loop*, International Journal of Thermal Sciences, pp. 1183 – 1192.

Author's contribution:

I: Boiling tests (Set-up design, conducting tests), writing of entire manuscript, analysis.

II: Boiling tests (Set-up design, conducting tests), writing of the boiling part of manuscript, analysis.

III: Boiling tests (Set-up design, building test equipment, conducting tests), fabrication of enhancement structure, writing of entire manuscript, analysis.

IV: Boiling tests (Set-up design, conducting tests), equal share in fabrication of enhancement structure, writing of entire manuscript, analysis.

V: Boiling tests (Set-up design, closely supervising the conducting of tests performed by Master thesis student: Yongtian Xu), writing of entire manuscript, analysis.

VI: Boiling tests (Set-up design, closely supervising the conducting of tests performed by Master thesis student: Yongtian Xu), R. Khodabandeh is main author of manuscript, equal share in analysis of the results.

Other publications not included in thesis

Rahmatollah Khodabandeh, Richard Furberg, 2010, *Instability, Heat Transfer and Flow Regime in a Two-phase Flow Thermosyphon Loop at Different Diameter Evaporator Channel*, Applied Thermal Engineering, Vol. 30, pp. 1107 – 1114.

Patent applications: "Porous layer", PCT/SE2007/000208 initial filing date: 3/3/06, application number: 0600475-8, authors: Furberg, R., Li, S., Mamoun, M., Palm, B., Toprak, M.).

1 Introduction

Why Enhanced Boiling?

Boiling heat transfer appears to be an area of research that doesn't raise many eyebrows at a dinner conversation. So why try to enhance this obscure phenomenon? In an attempt to answer this question, a number of benefits associated with enhanced boiling technology need to be mentioned.

Energy Efficiency - as engineers, we are often occupied with energy efficiency, and those of us, who are active in the field of heat pumping and refrigeration technologies, are no different. A reduction of the temperature difference in an evaporator or condenser by 1 °C translates into an improved energy efficiency of about 2-4%, dependent on the Carnot efficiency of the system. Considering that a five degree reduction could save us up to 20% in energy consumption and that billions of dollars are spent annually to power heat pumping machines, it's no wonder that there is an intense hunt for reductions in "delta T" (temperature difference). In enhanced boiling heat transfer, the goal is to reduce the temperature differences in evaporators by improving the mechanisms of heat transfer.

Miniaturization - many of us recall a time when cell phones would not fit into one's pocket, or when computers were the size of buildings? Space efficiency, or miniaturization, is one of the strongest incentives for technological development. Small components that can perform the same function as larger ones, are not only minimally invasive, but tend to come with a number of benefits apart from the obvious advantage of more efficient use of resources. If we can exchange the same amount of heat in half the space normally required, what can we not do with the volume that's freed up? Perhaps we could add new functions that formerly would not fit, lower the weight of the product and thereby finding new applications? The list of new opportunities could be endless. Miniaturization may also lead to favorable scaling laws when forces that scale with low exponential power become more prominent in the micro domain, e.g., surface tension forces become increasingly important compared to gravity forces in a narrower capillary. By the use of enhanced boiling, the same amount of heat can be transferred over a smaller volume or area.

Reliability and Safety - for cooling of increasing power dissipation from CPU chips and microprocessors, new and innovative heat transfer surfaces are continuously being developed and tested. Direct liquid cooling, involving boiling heat transfer, is one of the most effective ways to maintain a low component temperature and thereby assure a reliable operation of the unit. At very high heat fluxes, a regular boiling surface will transition into the film boiling regime (the so called critical heat flux, CHF) and thereby experience a rapid temperature increase of often several hundred degrees, if the heat flux is given. This would result in a breakdown of the electronic component, but with enhanced boiling techniques, the CHF can be increased and thus a continuous cooling of the component can be ensured. As we are acutely aware of, reliable and effective cooling in nuclear power reactors is of highest priority, where

transition to film boiling can have devastating consequences. Here, enhanced boiling techniques may increase the safety margin considerably.

Economic Efficiency – As alluded to above, the economic benefits of enhanced boiling can be very compelling and extend beyond the cost side of the business equation. There is a monetary value to all the advantages listed above; better energy efficiency, a more reliable product, new functionality, improved mobility, etc. These competitive advantages are often worth far more than the cost savings that would come from reduced use of material for a smaller heat exchanger.

As a result of these benefits, enhanced boiling technologies have made important inroads into the refrigeration and air-conditioning industries, the oil, gas and chemical processing industries, the microelectronics industry, the space industry, waste heat recovery for power generation (organic rankine) and several others.

Thesis at hand

The work presented here has its focus on passively enhanced pool boiling. The research project is a unique collaboration effort between the Division of Applied Thermodynamics and Refrigeration and the Functional Materials Group at the Royal Institute of Technology, in which research and competences from two different fields of science are combined and applied. Recent discoveries within both fields of expertise have made valuable synergies possible.

Developments within nano- and micro- technologies have made possible the creation of well structured surfaces down to the nano-scale, by template techniques and novel electrochemical deposition processes. Also, new findings have shown the importance of nano- and micro-sized features of the surfaces for the boiling performance of the surface.

The combination of these developments has opened up the possibility to explore the connection between the microscopic topology of the surface and the macroscopic boiling performance.

Objective

The overall research objectives of the doctoral thesis project were to:

- Develop methods for producing highly efficient micro- and nano-structured boiling surfaces.
- Study the microscopic nucleation behavior and the macroscopic heat transfer performance of the developed surface and relate the behavior to the structure of the surface.
- Use the developed methods and manufacturing techniques to produce highly efficient boiling surfaces suitable for exploitation in commercial equipment.
- Develop models for predicting the nucleation process and the boiling heat transfer performance of micro-structured surfaces from a geometric

description of the surface and known thermodynamic and transport properties of the fluid and the surface material.

Methods

Experimental methods have been used in developing a highly efficient boiling surface and the testing of its heat transfer performance. The development of a new surface structure consisted of testing several different ideas through visual observation of the fabricated surface in a scanning electron microscope (SEM), measuring the various structural and geometrical parameters, such as weight, porosity, pore-density, thickness, etc., and also experimentally measuring the mechanical stability of the surface structure. The boiling performance of the different surface structures was experimentally evaluated in two different pool boiling test rigs, a plate heat exchanger flow boiling set up and in a thermosyphon. High speed video system with a macro lens was also used to study the boiling phenomenon.

Due to the complexity of the boiling mechanism and the many interrelated physical phenomena, accurate pool and flow boiling models do not exist for neither plain nor smooth surfaces. But, the experimental results were used to develop a boiling model for the enhanced surface, in a first attempt at describing the boiling mechanism inside the porous structure.

2 Fundamentals of Pool Boiling

Boiling is when a substance changes phase from liquid to gas by being heated to the boiling point. This process could take place in a liquid that is either stagnant or moving relative to the heating surface, referred to as pool and flow boiling respectively. A simplified illustration in Figure 1 of the classical boiling curve for saturated pool boiling, with its relationship between heat flux, q'' and wall superheat relative to the saturated liquid, ΔT, serves as a good introduction to the area of enhanced boiling.

As heat flux is being applied to the surface, liquid density differences induce natural convection in the bulk liquid. No bubbles have yet been formed, instead evaporation takes place at the free liquid surface. Since natural convection is a relatively ineffective mode of heat transfer, the surface temperature increases rapidly when heat flux is increased.

At the onset of nucleate boiling, or boiling incipience, bubble generation is initiated on the surface. Due to surface tension forces at the vapor and liquid interface, the vapor pressure in a bubble is inversely proportional to the bubble radius. Therefore, the saturation temperature of the vapor inside the bubble is always higher than that of the liquid, which means that small bubbles require larger liquid superheat for evaporation to take place over the bubble interface. This is the reason why a certain hysteresis is observed at boiling incipience, even if small vapor embryos are trapped in the surface.

Due to the effective heat transfer that takes place around the bubble and the increased liquid agitation caused by the growing and departing bubbles, the surface temperature typically drops significantly at boiling incipience. By the trapping of uncondensed gases in a porous surface layer, or the presence of well suited nucleation sites, an enhanced surface may lower the wall superheat for onset on nucleate boiling. The benefit may be; more predictable behavior of a heat exchanger, reduced temperature overshoot which may damage components, especially electronic ones, or simply a better performing heat exchanger surface at low heat flux conditions.

After boiling inception, heat is transferred more effectively from the surface in the nucleate boiling regime, which may be seen in the increased slope of the curve. As the surface temperature increases, the nucleation site density and frequency increase and the initially isolated bubbles begin to merge laterally and vertically into vapor columns. In this nucleate boiling region, an enhanced boiling surface may provide various surface features that improve both heat transfer around the bubble and in the liquid, thus increasing the heat transfer coefficient, h, ($h = q''/\Delta T$).

As the heat flux increases further, vapor patches start to grow and form on the surface which is periodically rewetted by surrounding liquid. This limits the effective liquid evaporation that is taking place around the bubbles and leads to a reduced curve slope. At the critical heat flux (q''_{CHF}), the vapor flow prevents liquid rewetting and the surface becomes covered in a vapor film resulting in a rapid and large temperature increase, if the heat flux is constant. The high surface temperature may result in melting of the surface material or the heating element. An enhanced boiling surface may delay this transition into film boiling, by for instance separating the vapor columns and thus enabling larger heat fluxes to be transferred through the heat exchanger surface.

The boiling curve often takes on a different shape as the heat flux is decreased from a high level, so called boiling hysteresis. For instance, the nucleate boiling regime may often be sustained at low temperature differences where only natural convection was occurring at increasing heat flux. Further, a stable film boiling regime can be observed between the critical heat flux and the minimum film boiling heat flux (q''_{MFB}). As the heat flux is further reduced below the minimum film boiling point, the vapor film collapses and a quick transition to nucleate boiling occurs, resulting in a significant temperature drop.

Thus, enhanced boiling surface may affect one or more of these aforementioned boiling characteristics; lowering the temperature at onset of nucleate boiling; improving the heat transfer coefficient in the nucleate boiling regime; increasing the critical heat flux. This thesis work will primarily be focusing and covering the relationship of enhanced surface features and the related heat transfer mechanisms in the nucleate boiling regime.

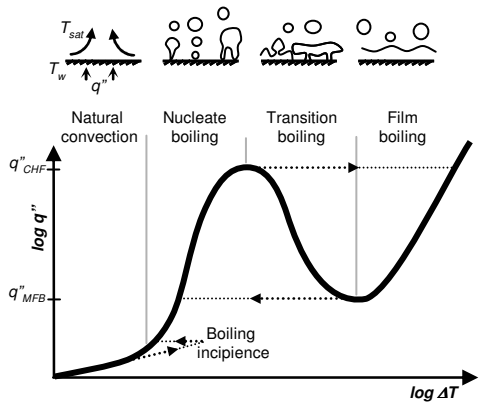

Figure 1. Boiling curve for saturated pool boiling.

Pool Boiling Heat Transfer Mechanisms

Different heat transfer mechanisms are involved in pool boiling and theoretical models have been developed to describe these mechanisms. The main mechanisms could be summarized in different categories; microconvection, micro-layer evaporation, three-phase-line evaporation and transient conduction into superheated liquid layer. These various heat transfer mechanisms often take place simultaneously and interdependently around the bubble and are affected by surface characteristics, fluid properties and the interaction between surface and fluid.

Various forms of pool boiling heat transfer mechanisms are illustrated in Figure 2. Initial bubble nucleation occurs when the first liquid molecules change phase to vapor. The nucleation phenomenon is complex and not within the scope of this thesis. Initial bubble generation occurs when the liquid surrounding vapor or gas trapped in a cavity is superheated enough to overcome the surface tension force, according to the classical theory by Hsu (1962). After initial bubble generation, liquid evaporation at the liquid/vapor interface causes the bubble to grow. Natural convection is driven by density differences in the liquid which are caused by the heating wall, whereas microconvection is the liquid motion caused by growing and departing bubbles. Thus natural convection and microconvection are single-phase heat transfer mechanisms between the heated surface and the liquid.

Micro-layer evaporation refers to the evaporation heat transfer of the thin liquid film that is formed under a growing bubble. The liquid wedge is formed due to the interaction of liquid inertia and surface tension forces. The latent heat needed to evaporate the liquid comes from the superheated wall. The bubble may also grow through evaporation over the bubble dome as the latent heat is transferred from the superheated liquid layer surrounding the bubble. If the bubble grows out of the superheated liquid layer, vapor condensate into liquid at the bubble cap, thus transporting heat from the bubble to the liquid.

Evaporation may also take place along the three-phase line. The meniscus in the vicinity of the contact line can become very thin, resulting in high heat transfer in this region. The adsorbed layer is usually just a few molecules thick and cannot be evaporated due to molecular adhesion forces. High heat transfer may

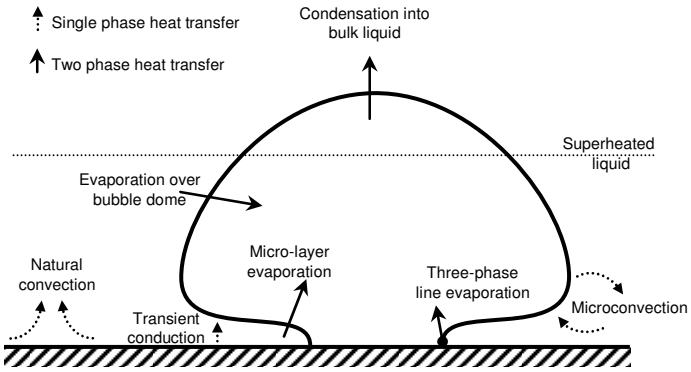

Figure 2. Heat transfer mechanisms during nucleate boiling.

take place when the film is thick enough such that the adhesion forces become small, yet thin enough so the heat conduction through the film is high. As the bubble grows, the buoyancy forces increase and eventually the bubble departs. As the three-phase line recedes and the bubble necking process starts, the same heat transfer mechanisms may take place as during the main growth phase for the bubble. If the micro-layer has completely, or partially, evaporated during bubble growth, the dry surface will be rewetted as the bubble departs. Heat is transferred into the advancing liquid front as the dry patch underneath the bubble is rewetted. This rewetting of the surface is often referred to as transient conduction, where heat is stored in the surface material underneath the bubble during the growth period and transferred to the liquid during the bubble departure process; see for instance Demiray et al. (2004).

Several studies emphasizing the different pool boiling mechanisms have been conducted throughout the last decades. Cooper and Lloyd (1969) used micro-thermocouples and high speed cine films to study the surface temperature under a growing bubble. The energy for the bubble growth was calculated to come solely from micro-layer evaporation. The results gave support to the, then fairly new, micro-layer theory. Wayner et al. (1976) in a study fundamental to the theoretical thin film evaporation concept, developed a mathematical model for the average heat transfer coefficient for the interline region, or three-phase line, between vapor, liquid and surface of an adsorption controlled wetting film. Later, Stephan and Hammer (1994) suggested a boiling model where heat is transferred through the three-phase contact line and micro-layer evaporation of a growing bubble. Capillary pressure, curvature effects, adhesion forces and liquid transport were included in the so called micro-region model. Results were compared to experimental boiling tests and the micro region was found to be less than 1 μm long, but accounting up to 60% of the total heat transfer. A peak heat flux 100 times larger than the CHF was observed within the micro region.

To lend further support to the importance of the three-phase contact line evaporation, Höhmann and Stephan (2002) used temperature sensitive liquid crystals (TLC) and two high-speed digital cameras in conjunction with a microscope to investigate the heat transfer at an evaporating liquid meniscus, with a resolution of less than 1 μm. The data obtained, showed high heat flux in the micro-region of the meniscus. Mitrovic (1998, 2002) attempted to show analytically that the heat and energy transformation, associated with bubble growth, are concentrated along the TPL (three-phase line) of concave-convex curvature of the interface due to evaporation along the line. Surface roughness influences the boiling process by augmenting bubble nucleation and increasing nucleation site density, but surface roughness would also result in longer TPL, thus improving the heat transfer.

Mikic and Rohsenhow (1969) presented a boiling model where the departing bubble removes the superheated liquid layer surrounding the bubble over an area twice the bubble departure diameter. After bubble departure, colder bulk liquid flows into contact with the surface. The superheated layer is thought to be renewed during the waiting time between bubble departure and bubble nucleation. Kim (2009) labels this as transient conduction, since convection into the bulk liquid after bubble departure was assumed to be the dominant mode of heat transfer.

This quick overview of heat transfer mechanisms illustrate that boiling is a multi-scale dependent phenomenon where the heat transfer mechanisms are affected by surface features on both macro-, micro- and nano-level. Recent advancements in measurement technologies and computational fluid dynamics have made it possible to study the boiling phenomena with very high spatial and temporal resolution. Typically, these measurements are performed on idealized flat surfaces, but a deepened understanding of the boiling phenomena aids and guides the development of enhanced boiling structures.

Triggered by findings by Yaddanapudi and Kim (2001), who studied single bubbles growing on a constant temperature micro heater array and who found that over 40% of the latent energy came from heat transferred through the bubble dome (the rest, 60% through the liquid micro-layer), Liao et al. (2004) developed a physical model for early stage bubble growth in saturated nucleate boiling. It was found that the thin unsteady thermal boundary layer near the rapidly growing bubble allows for significant amount of heat flux from the bulk liquid to the vapor dome, which in some cases can be larger than the heat transfer from the micro-layer. Refining the approach with micro heaters, Demiray et al. (2004), Myers et al. (2005) and Kim (2009) reported on a new experimental heater configuration of 10x10 micro-heaters, each with 100μm resolution, see Figure 3. The tests were conducted in FC-72 at atmospheric pressure and the set-up allowed direct heat transfer measurements under nucleating bubbles, combined with high-speed digital video imaging. For a constant temperature heater array; the bubble draws most of its energy from the superheated liquid layer surrounding it, where conduction and micro-convection are the mechanisms though which this energy is replenished. For a constant heat flux arrangement; transient conduction/micro convection, during liquid rewetting of the surface, accounted for most of the wall heat transfer. Bubble coalescence only had a small impact on the heat transfer rate.

Mohaddam and Kiger (2008) reached similar conclusions when they performed high resolution (20-40μm) thermal field measurements under isolated bubbles in FC-72, see Figure 4. A set of temperature sensors within and on the surface of the composite wall were designed to measure the temperature of the wall surface, both beneath the bubble on the liquid–solid interface, as well as on the interior boundary within the composite solid. They found that micro layer heat

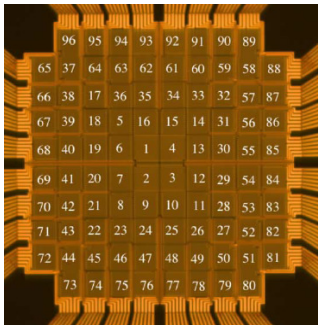

Figure 3. Photograph of the 100 microheaters, each 100x100 μm.(Myers et al., 2005)

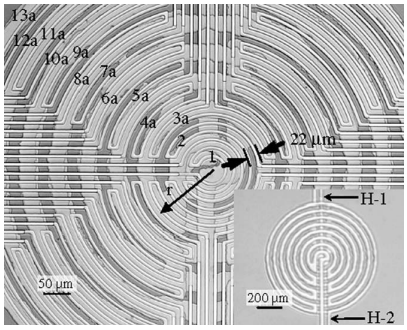

Figure 4. Close view of device showing sensor array. (Mohaddam and Kiger, 2008)

transfer accounted for about 16-29% of total heat transfer and transient conduction and micro convection was the dominating heat transfer mechanisms. Further, they concluded that evaporation at the three-phase contact line it was about 2–3 orders of magnitude less than their measured heat transfer and was therefore negligible. The influences of the various mechanisms were dependent on the surface temperature.

Wagner and Stephan (2009) employed an infrared camera to measure the temperature distribution on the backside of a 20 μm thick stainless steel heating foil during boiling of FC-84 and FC-3284. The bubble shape was also imaged from the side, making it possible to calculate the total latent heat transfer into the growing bubble. The micro region heat flux varied through the bubble growth period and was found to be highest during the initial explosion like bubble growth phase and during bubble detachment with advancing contact angle. For pure fluids, Wagner and Stephan reports that up to 50–60% of the latent heat was found to flow through the micro region. As pointed out by Kim (2009), the heat transfer through the wall under the bubble between nucleation through bubble departure is about 22% of the total bubble latent heat in the results reported by Wagner and Stephan (2009). Thus, the Wagner and Stephan (2009) results appear to be in quite good agreement with those of Demiray et al. (2004), Myers et al. (2005), Kim (2009) and Mohaddam and Kiger (2008).

Boiling heat transfer is a function of a multitude of interrelated sub-processes such as: bubble dynamics, fractional area of liquid-solid contacts and their duration, mechanisms of heat transfer, interfacial instabilities, and interfacial mass and heat transfer as well as other independent variables such as; heater size, shape, thickness and surface condition, heating method, liquid temperature, systems pressure, liquid and vapor thermo-physical properties, heater confinement, and flow conditions. Since these sub-processes are interrelated, the global model will only work if the processes are modeled simultaneously, and because of the profound complexities involved, numerical computer simulations are necessary. Currently, with the rapid improvement in the numerical capabilities and processing speeds of computational fluid dynamics, we are getting closer to the objective of reaching a complete understanding of boiling heat transfer.

Dhir (2001 and 2006) presented two-dimensional numerical simulations of both

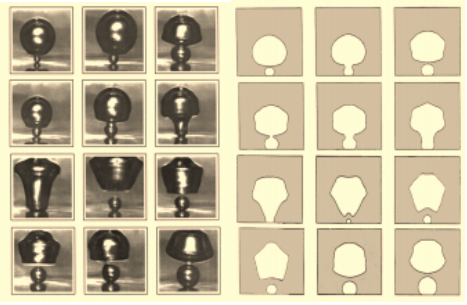

Figure 5. Bubble merger normal to the heater. (Dhir, 2001)

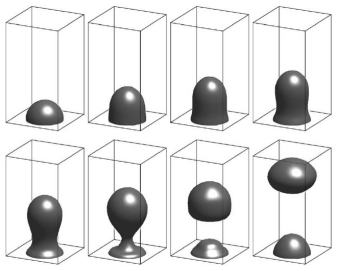

Figure 6. Interface plots for a three-dimensional nucleate boiling simulation. (Shin et al., 2005)

pool nucleate and film boiling, including both the macro- and the micro region of the growing bubble and complete solutions to the conservation equations of mass, momentum, and energy for liquid and vapor phases at and near a heated surface. The simulations were validated with experimental measurements of heat transfer rates, bubble release pattern, bubble shape and the interface growth rate and found to be remarkably accurate, see Figure 5. About 20% of the total heat transfer was found to have come from micro-layer evaporation. The simulations showed accurate results for nucleate boiling pertaining to the effects of; wall superheat, contact angle, liquid subcooling, level of gravity, heat transfer rates, bubble merger and formation of vapor columns.

Shin et al. (2005) performed a full direct numerical simulation of nucleate boiling in a fully three-dimensional geometry using the level contour reconstruction method, which was developed by Shin and Juric (2002). The effect of nucleation site density and the interaction with other bubbles were included in the model and it was found that the bubble's effect on neighboring bubbles was important for predicting the proper relationship between heat flux and the wall superheat in a realistic surface. The micro-layer evaporation and contact line dynamics beneath the bubble was not included in the model. The contact region was approximated as fixed in spaced, which can be seen in Figure 6. The three-dimensional simulations, including the effect of neighboring bubbles, showed better agreement with some known pool boiling correlations, than two-dimensional simulations did.

As a summary, the aforementioned experimental studies, as well as computational simulations by Dhir (2001 and 2006) indicate that for a constant temperature heater array, the bubble draws most of its energy from the superheated liquid layer surrounding it, where conduction and micro-convection are the mechanisms through which this energy is replenished.

These types of fundamental studies are valuable for our basic understanding of the boiling phenomenon. But, it is important to keep in mind under which conditions these experiments were conducted; extremely smooth surfaces, thin surface layers and single bubbles. In most industrial applications, heaters are thick, many bubbles interact and the heater surface either has a surface roughness or a structure, in the case of enhanced boiling. Since, enhanced boiling is the focus of this thesis work, next chapter will review the boiling performance and mechanisms in various enhanced structures.

3 Surface Structures for Enhanced Boiling

The following chapter contains a review of the literature on a wide variety of enhancement structures, from those where the millimeter scale is determining the boiling behavior, to the most recent micro- and nanostructures, which have been reported on during the past few years. For a more comprehensive literature review of the research within the field of enhanced boiling, the reader is referred to a literature survey by Furberg (2010). The chapter is organized along different surface structures; machined structured surfaces, wire or mesh structures, porous particle layers, porous particles layers with designed features, porous materials and designed nano- and microstructures.

There are several ways in which to improve the boiling performance and characteristics of a heat transfer surface. The main distinction is usually made between passive and active techniques. To augment boiling, passive techniques employ special boiling surface geometries, or fluid additives, such as; roughening of the heat transfer surface, pitting the surface with corrosive chemical, integral fins or rolling, coating the surface with a porous layer, or the fluid additives that alters the surface tension of the liquid. Active techniques need external power, such as electric or acoustic fields and surface vibration. Most of the active techniques have proven to be difficult to realize outside the laboratory or to justify economically, while the passive ones have found their way into different engineering applications.

Both the area of fundamental boiling research and that of passive boiling enhancement technology have been subject to interesting developments during the last couple of years. To a large extent, advances in the field of micro- and nano-technology have facilitated this development. Miniaturization technology has made possible the fabrication of experimental boiling surfaces scaled to the size of bubbles and with enhancement features, controlled down to the level of nanometers. As presented in the previous chapter, some of these surfaces have integrated temperature sensors and heaters, and in combination with high speed imaging systems and computational fluid dynamics, important advances in understanding of the fundamental boiling mechanisms have been made.

None of us have been able to escape the reports on the emergence of nanotechnology, where materials, structures or devices are given new properties by means of controlled manipulation of their microstructure at the atomic or molecular level. Now, when nano-size building blocks can be arranged into high dimensional structures with controlled interfaces, new, and very promising surface structures can be manufactured for enhanced boiling applications.

Machined Structured Surfaces

Nakayama et al. (1980) and (1982), were the first to visualize the pool boiling process inside a porous enhancement structure, consisting of interconnected tunnels with small pores connecting the tunnels and the pool liquid, see Figure 7. The visual observations suggested that the pumping action of departing bubbles was sucking liquid into the tunnel. Capillary forces were spreading the introduced liquid in angled corners, and subsequent evaporation of the liquid formed another generation of bubbles. A dynamic explanation model; the so called liquid suction-evaporation model, was developed to simulate the heat transfer from the structure, as illustrated in Figure 8. The experimental data show a significant contribution of latent heat transport from the structure, compared to a plain surface. Ramaswamy et al. (2002), (2003) and (2005) used the Nakayama suction-evaporation model to fairly successfully predict the bubble departure diameter, frequency, and nucleation site density from enhanced structures consisting of micro-channels on a silicon wafer with various channel depth, pitch, and height, as seen in Figure 9. High-speed visualization imagery was used to study the pool boiling at atmospheric pressure in FC-72.

Working with a similar structure, but also testing it with a top cover, Ghiu and Joshi (2005) used a high speed camera to visualize the pool boiling dynamics in PF500 (dielectric). The heat transfer performance of the top covered structure is

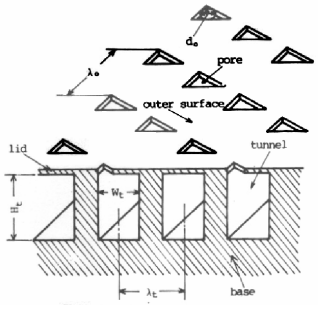

Figure 7. Geometry of the surface structure, including top- and cross-sectional views. (Nakayama et al., 1980)

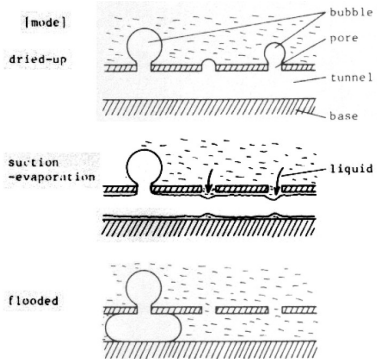

Figure 8. The dynamic liquid suction-evaporation model. (Nakayama et al., 1982)

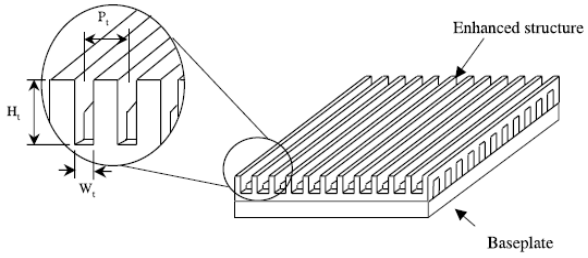

Figure 9. Enhanced structure in silicon, copper and quartz. (Ramaswamy et al. 2002)

significantly less than that for open top structures, due to the reduction of external convection, which accounted for about 70% of heat transfer in the similar structure of Nakayama et al. (1980). The oscillatory movement of the vapor/liquid interfaces was confirmed as one of the main characteristic of the liquid/vapor dynamics inside the enhanced structure. Another conclusion from the study is that the internal evaporation process is an important heat transfer mechanism with a significant contribution to the total dissipated heat. Results indicated that the evaporation through the liquid meniscus that forms in the corners of the matrix was an important heat transfer mechanism.

Pastuszko (2008) studied boiling heat transfer on structured surfaces covered with perforated foil, forming sub-surface tunnels, very similar to commercial tube enhancement structures, such as Wieland GEWA-TW and Hitachi Thermoexcel-E, see Figure 10. Several parallels also exist with the Nakayama (1980, 1982) structures. The effects of hole-diameters, tunnel pitch and width were examined and enhancements of about a 2-4 times, compared to a smooth finned surface, were recorded. The conclusion was drawn that the evaporation within the tunnels and convection on their external surfaces had a determinative effect on the heat transfer coefficient, see Figure 11. Das et al. (2009) tested the

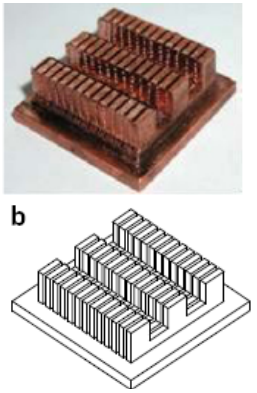

Figure 10. Copper structure overlaid with perforated foils and vertical and horizontal cross-sections. (Pastuszko, 2008)

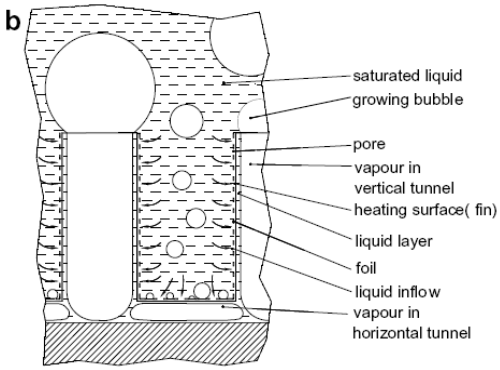

Figure 11. Joined tunnels vertical cross-section: liquid inflow and bubble generation sites. (Pastuszko, 2008)

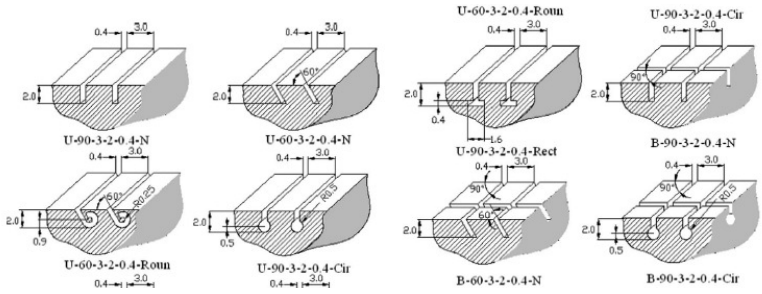

Figure 12. Surface structures with parallel or orthogonally intersecting tunnels and different cavity structures at tunnel base. Das et al., (2009)

boiling performance of different surface structures with parallel or orthogonally intersecting tunnels, as seen in Figure 12. The effect of design parameters like tunnel inclination and different cavity structure at the tunnel base on the boiling heat transfer was investigated. The highest augmentation was obtained from the surface having intersecting inclined tunnels with a circular base.

Wire and Mesh Structures

Li and Peterson (2007) fabricated porous surfaces out of sintered copper wire mesh, see Figure 13, and studied the boiling performance in water at atmospheric pressure, by varying the layer thickness, porosity, pore size, surface conditions of the structure and the heater to coating thickness ratio. It was found that nucleate boiling and evaporation, both occur inside of the porous media and that stable internal vapor and liquid counter-flow patterns are formed in thick porous coatings during the boiling process. A thin vapor film is often formed near the heating wall on thick coatings, depending on the magnitude of the heat flux – evidence of this was found in the experiments. Boiling performance and characteristics were strongly dependent on the geometric parameters, the thermal properties of the porous media, and the contact conditions between the porous coatings and the heated wall. Porous coatings with higher thermal conductivity were found to perform better than those with lower thermal conductivities, especially at low heat fluxes. Two different types of vapor ventilation mode was identified; liquid-vapor countercurrent flow, where the vapor escapes upward and the liquid flow is in the opposite direction driven by the gravity with partial assistance of capillary pressure, and liquid-vapor separating flow, where the major vapor vents through the vapor channel formed near the heater wall to the unsealed sides and the liquid enters the porous coatings from the top.

Franco et al. (2005) tested the boiling characteristics, including CHF, of metallic mesh structures in the dielectric refrigerant R141b under atmospheric pressure. The effectiveness of the mesh structure depended on wire material, net aperture, wire diameter and number of layers. Optimum combination of number of layers, wire diameter, and mesh aperture was found. CHF could be further improved by placing finer wire net on the heated surface and larger wire nets on the upper levels, creating conical vapor escape channels.

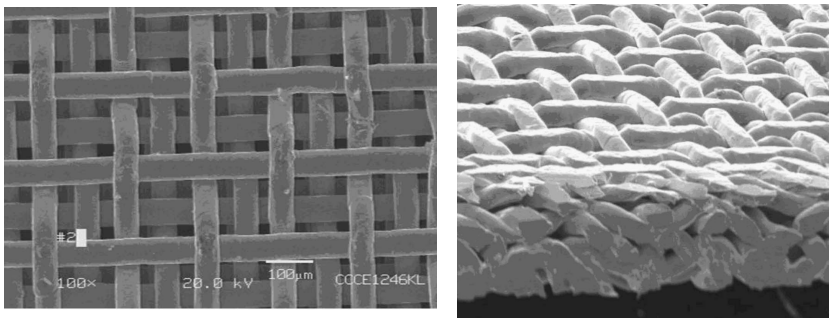

Figure 13. Top and side view of images of sintered isotropic copper mesh with 1509 m^{-1}, 56 µm wire diameter. (*Li and Peterson, 2007)*

Porous Particle Layers

Since the introduction and commercialization of the High-Flux surface by O'Neill et al.(1971) and due to the relative simplicity in manufacturing, enhanced boiling in porous particle layers have been studied quite extensively. Scurlock (1994) tested the pool boiling performance of surfaces of various thicknesses of plasma spayed porous aluminum and aluminum/silicon coatings in liquid nitrogen, argon, oxygen and R12. It was found that there is an optimum thickness for each liquid and selected heat flux. At low heat flux, the boiling curves for the four liquids were distinct, demonstrating that the boiling characteristics are governed by the fluid properties. At higher heat fluxes, the curves merge into a common curve which is believed to mean that the thermal conduction of the coating dominated the heat transfer. The general trend is that thicker structures perform better at lower heat fluxes, but thinner structures perform better at higher heat fluxes. Two different boiling regimes were suggested as an explanation for this behavior; base and surface boiling. Base boiling (at low heat flux) occurs when the porous coating is fully flooded and liquid boiling takes place in contact with the substrate metal. The vapor escapes through the numerous channels in the coating with little impedance. At higher heat flux, the liquid is pushed out of the porous coating by a vapor blanket and boiling takes place at the surface of the coating and heat transfer is only limited by the thermal conductivity of the porous metal matrix.

You et al., at University of Texas at Arlington, have published a series of articles based on their research on a micro-porous aluminum, copper, silver and diamond particle coating, see Figure 14. O'Connor and You (1995) presents pool boiling experiments in FC-72 from five enhanced structures of various thicknesses, varying from 23 to 124 μm, consisting of 3-10μm large silver flakes epoxy-bonded to a surface. A significant reduction in nucleate boiling superheats, decrease in incipience superheat, and an increase in CHF was recorded.

Chang and You (1997) studied particle size effects on boiling performance of micro-porous enhanced surfaces using five different sizes of diamond particles. By comparing the coating thickness with a calculated superheated liquid layer thickness of about 100 μm, the coatings are classified into two groups: 'micro-porous' and 'porous' coatings. Micro-porous coating shows different

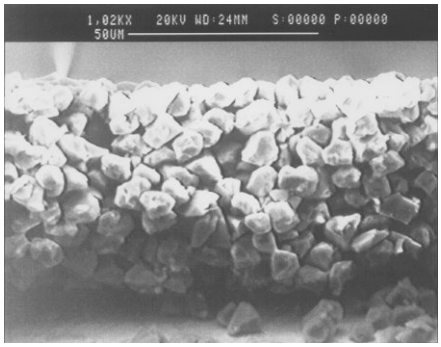

Figure 14. SEM Image of surface micro-structure of diamond particle coating. (Kim et al., 2002)

characteristics of boiling performance compared to porous coating in incipient superheat, nucleate boiling and CHF. At higher heat fluxes, thicker layers had a lower heat transfer performance compared to thinner ones, which was believed to be due to higher impedance for liquid-vapor exchange channels. The liquid supply to the innermost active portion of the porous coating is hindered due to additional hydraulic resistance over liquid-vapor exchange channels, reducing cooling performance. Further, higher thermal resistance due to increased coating thickness and low thermal conductivity in the particle layer, resulted in an increase in temperature drop at higher heat fluxes.

Chang and You (1996) also investigated the heater orientation effects of the micro-porous enhanced surface under saturated conditions in FC-72. The nucleate boiling superheats of the micro-porous surfaces were independent of orientation. This behavior was attributed to the presence of active nucleation sites over the entire heater surface regardless of orientation angle. CHF decreased with increasing orientation angle (horizontal surface facing up: 0°). In contrast, the nucleate boiling superheats of plain reference surfaces were lowered at increasing heater orientation angle.

Rainey and You (2000) investigated the nucleate boiling heat transfer and CHF of a combination of pin fin arrays (height: 1 - 8 mm) and a micro-porous coating. The application of micro-porous coating significantly improved the heat transfer coefficient, while the CHF was not affected by the micro-porous structure, except in the case of the surface with 8 mm long fins. The nucleation boiling and CHF behavior were found to depend on multiple, counteracting mechanisms such as surface area enhancement, fin efficiency, surface micro-structure, vapor bubble resistance, and re-wetting liquid flow resistance. Rainey and You (2001) also tested the effects of heater size (1x1, 2x2, and 5x5 cm) and orientation (0°, 45°, 90°, 135°, 160°, 190°) from a micro-porous surface. The nucleate boiling performance of plain surfaces was dependent on heater orientation, but this was not the case for the micro-porous surface. The effects of heater size and orientation angle on CHF were found to be significant for both plain and micro-porous surfaces.

Kim et al. (2002) investigated the boiling heat transfer mechanism of micro-porous surfaces in saturated FC-72 by measuring the bubble size, frequency, and vapor flow rate from a plain and micro-porous coated 390 μm diameter platinum wire. It was found that the improved performance of the micro-porous coating came from increased latent heat transfer in the low heat flux region and from increased convection heat transfer (sensible heat) in the high heat flux region. The critical heat flux for the micro-porous coated surface is enhanced over the plain surface due to decreased vapor generation rate and perhaps also due to increased hydrodynamic stability from increased vapor inertia, as a results of increased nucleation site density.

Hwang and Kaviany (2006) experimentally tested the CHF for uniform porous coatings of different type of copper particles (40-80μm). CHF was found to be independent of particle size, particle features and porous layer preparations. The authors also draw some interesting conclusions from the boiling performance at moderate heat flux. Evaporation is believed to take place at the interface of thin liquid films covering the particles. The contact resistance between the structure

and the heated surface is considered important as well as the thermal conductivity of the structure.

Yang and Liu (2008) tested the pool boiling heat transfer performance in methanol of a vertical surface, coated with an 180μm thick micro-porous aluminum particle structure, in a 1 mm confined space. For the smooth surface the confinement had a positive heat transfer effect other than at highest heat flux. Unlike to the smooth reference surface, the confinement had a rather insignificant effect on the micro-porous surface, except for at high heat flux, where large amount of bubbles were confined by the cover plate, causing partial dry out.

Kim et al. (2008) investigated the pool boiling heat transfer characteristics in the dielectric liquid, PF5060, the effect of surface orientation and subcooling of three different types of enhancements on a copper substrate; sandpapered, etched micro-fins and a 45μm thick micro-porous coating, identical to that of O'Connor and You (1995). Inclined surfaces performed better and subcooling resulted in correspondingly lower surface temperatures. The micro-porous surface showed the highest heat transfer augmentation of up to 3 times that of a plain reference surface.

Porous Particles Layers with Designed Features

Liter and Kaviany (2001) tested porous coatings of spherical copper particles organized into various formations, as seen in Figure 15 and Figure 16 and found that CHF could be enhanced up to 3 times in pentane. The modulation of the particles is thought to separate the liquid and vapor phases, thus reducing the liquid-vapor counter-flow resistant adjacent to the surface. A theoretical model is presented, which quite accurately predicts the CHF for the various geometries tested.

Min et al. (2009), performed extensive parametric testing of several 2-D and 3-D porous stack-like structures, see Figure 17 and Figure 18. The structures were fabricated with a novel hot-powder compaction method. The heat transfer performance, particularly the CHF, for different height, width, pitch (modulation wavelength), particle diameter and porosity, was tested. The best 2-D and 3-D structures enhanced the CHF by a factor 3.3 and 2 respectively. The experimental results agree well with hydrodynamic stability theory and CHF was found to be mostly dependent on modulation wavelength. Porosity and particle diameter had only a small effect on CHF.

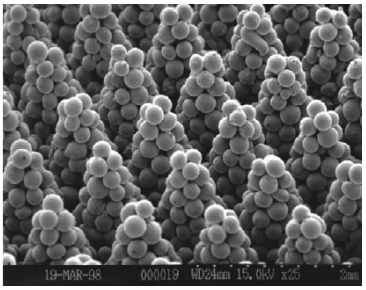

Figure 15. Spherical copper particles of 200μm diameter molded into conical stacks. (Liter and Kaviany, 2001)

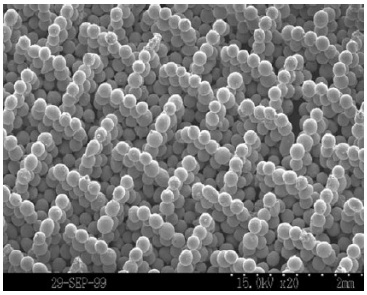

Figure 16. Spherical copper particles of 200μm diameter molded into tapered walls.(Liter and Kaviany, 2001)

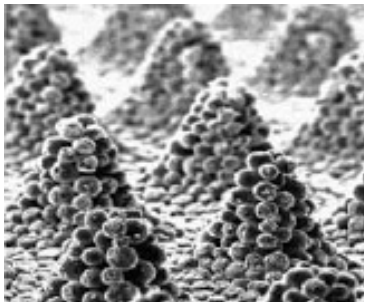

Figure 17. 3-D porous stacks made out of copper particles. (Min et al., 2009)

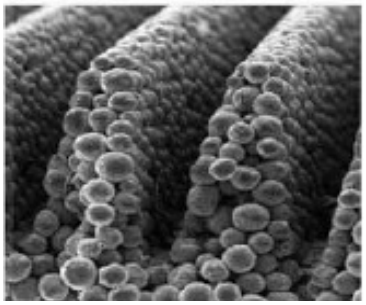

Figure 18. 2-D porous stacks.(Min et al., 2009)

Porous Materials

El-Genk and Parker (2005) investigated the boiling performance of porous graphite, see Figure 19. The porous graphite (1.6mm thick) is characterized by a volume porosity of 60% with cavities ranging from a few to hundreds of microns. Boiling incipience, heat transfer coefficient (16 times) and CHF (60%) were all significantly improved. Parker and El-Genk (2006) further studied the effect of surface orientation of the porous graphite in FC-72. The results show higher heat transfer coefficient and CHF for the porous graphite compared to that of a smooth copper surface under all inclinations.

Xu et al. (2008) studied the heat transfer boiling performance in acetone, using high speed video, of open celled copper foams with various mesh size, thickness and porosity, see Figure 20. The mesh size was found to have an important effect on the thermal performance. Large mesh size foams have better thermal performance at low surface superheats, but small mesh size foams have better one at moderate or large surface superheats. Larger foam cover thickness enhanced nucleate boiling heat transfer due to the increased bubble nucleation

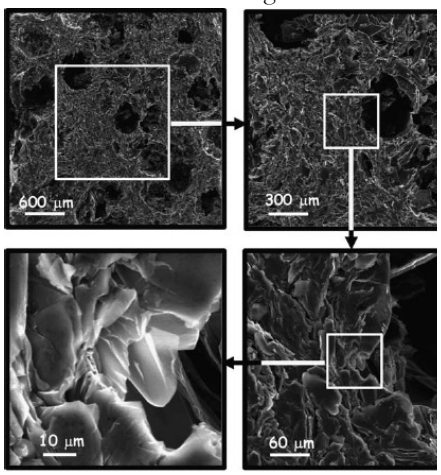

Figure 19. SEM images of the porous graphite surface. (El-Genk and Parker, 2005)

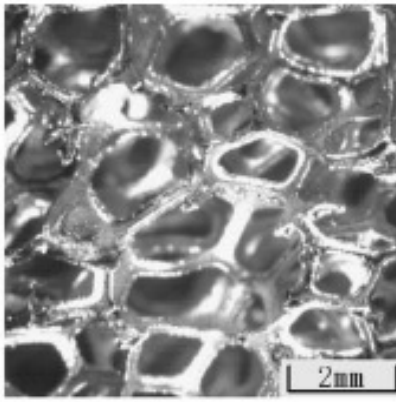

Figure 20. Open celled copper foam structure used for boiling enhancement. (Xu et al., 2008)

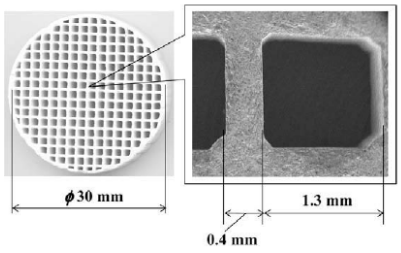

Figure 21. Shape of porous honeycomb plate. (Mori and Okuyama, 2009)

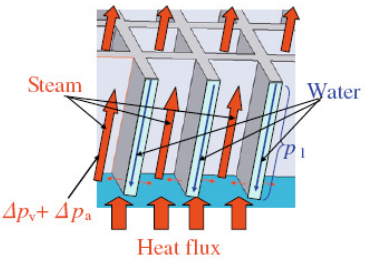

Figure 22. Vapor and liquid flow in porous honeycomb plate. (Mori and Okuyama, 2009)

site density at medium heat flux, but decreased heat transfer performance due to the increased resistance to vapor release at high heat flux.

Mori and Okuyama (2009) attached a porous ceramic honeycomb-structured plate, see Figure 21, to a heater to study the effect on CHF in saturated water. The ceramic material had low thermal conductivity and was only placed upon the heater surface and held in place with a wire mesh. The thickness of the plate was varied between 1.2, 5, and 10 mm. A honeycomb structure with the same dimensions, but without the porous wall structure as well as a porous plate without the vapor escape channels, were also tested (5 mm thickness). CHF was inversely proportional to the plate thickness. The CHF of the 1.2 mm thick plate was found to be up to 2.5 times higher compared to that of a plain surface. Automatic liquid supply due to capillary action and reduction of the flow resistance for vapor escape due to the separation of liquid and vapor flow paths by the honeycomb-structure were verified to play an important role in the enhancement of the CHF, see Figure 22. A simple model was developed to explain the impact of structure parameters such as wall porosity, layer thickness and vapor escape channel widths.

Designed Nano- and Microstructures

Honda et al. (2002) and Wei and Honda (2003) published the first studies on the effects of micro-pin fins and submicron-scale roughness on the boiling heat transfer from a silicon chip in FC-72, see Figure 23 and Figure 24. The most interesting result was that submicron-scale roughness further improved the enhancement for both the plain and the pin-fin chips. Hence, it was confirmed that nano-scale surface features affect the boiling heat transfer mechanisms. Furthermore, a high-speed video study of the boiling phenomena revealed that small amount of vapor was left within the gap between the pin fins when a growing bubble left the surface, which suggested that the evaporation that occurred within the small gap was responsible for the sharp increase in the heat flux with increasing wall superheat. A vertically mounted chip performed better than a horizontally oriented chip in the low flux region, the same in the medium heat flux region, but had a lower CHF.

The boiling behavior of the micro-pin-finned chips was characterized by an almost vertical boiling curve in the nucleate boiling region. With a uniform surface roughness for all fins, a regular geometry and the fact that all micro-pin-

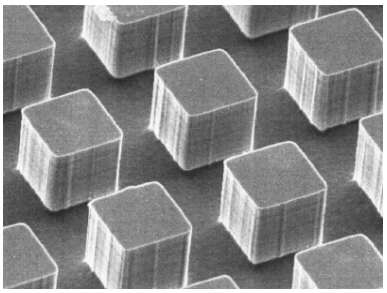

Figure 23. SEM picture of Chip with micro-pin fins. (Honda et al., 2002)

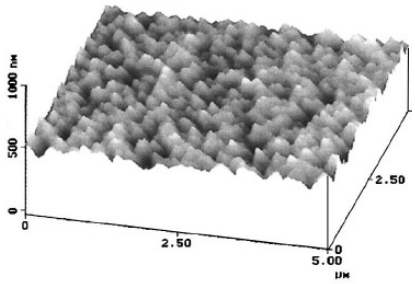

Figure 24. Atomic-force-microscope image of Chip with surface roughness (rms) 32.4 nm. (Honda et al., 2002)

fins are completely submerged in the layer of superheated liquid, the condition for bubble nucleation will be satisfied at almost the same temperature difference at all parts of the chip surface. Hence, the number of nucleation sites will increase rapidly as the temperature difference increases, thus resulting in nearly isothermal behavior (a vertical boiling curve).

Yuan et al. (2009) and Ma et al. (2009) tested the sub-cooled flow boiling performance, under various flow velocities in FC-72 of the same silicon pin-fin geometry as Wei and Honda have studied. The micro-pinned structure showed an enhancement of both the heat transfer coefficient and CHF, compared to a smooth silicon surface. The nucleate flow boiling curves for the two micropin-finned surfaces converged into one line indicating insensitivity to fluid velocity and subcooling. On the other hand, the CHF values were found to increase with fluid velocity and sub-cooling. Vemuri and Kim (2005) reported on pool boiling experiments from a nano-porous surface in FC-72. A 30% reduction in temperature superheat required for boiling incipience was found. The pore size of the structure was in the 50-250 nm range and the thickness of the structure was 70μm. The structure, an aluminum membrane filter was glued to the heated surface. These findings further indicate that even nano-sized pores may trap vapor patches and thereby lower the incipience boiling point.

Launay et al. (2005) has further modified the micro-porous silicon structure tested by Ramaswamy et al. (2002) with a coating of carbon nanotubes (CNTs) and thereby created a hybrid micro-nano structure for boiling enhancement. Tests were conducted in PF5060 and in deionized water. The surfaces tested were; smooth and roughened silicone surfaces, bare and fully coated with CNTs a silicon etched pin-fin array as well as a CNT-based pin-fin array, and 3-D structures with and without CNTs, see Figure 25. The conventional silicon fin-pin microstructure and the 3D microstructures showed the best performance. The CNT-enabled structures only improved boiling at low superheats. It was observed that the boiling curves for the CNT-based structures were similar to boiling curves exhibited by hydrophobic surfaces. An interesting comparison is that Honda et al. (2002) recorded an enhancing effect from the nano-roughness at all heat fluxes and not only at low heat flux.

Akapiev et al. (2003) and Schulz et al. (2005), were the firsts to present a geometrically well-defined microstructure with cylindrical copper whisker with a porosity of 75 to 99%, Figure 26. The structure was fabricated by a deposition process with a perforated foil as a mask. Mitrovic and Hartmann (2004)

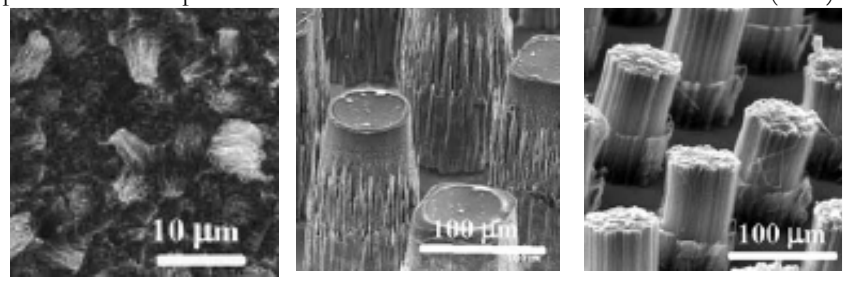

Figure 25. (Left). SEM of smooth sample covered with CTNs. (Middle) SEM of the silicon pin-fin structure. (Right) SEM of the carbon nanotube pin-fin array. (Launay et al., 2005)

conducted pool boiling tests of this microstructure in R141b. The boiling incipient point was lower and the heat transfer coefficient was improved over the whole heat flux range with approximately a factor 2 compared to the plain reference surface. An interesting observation was that the structure showed an isothermal behavior at varying heat flux, in the fully developed boiling region. Mitrovic (2005) speculates that the required properties of a surface structure with isothermal boiling behavior must be that of identical elements which are arranged in a mono-pattern on the heating surface. The structure elements (protrusions) must trap vapor after bubble detachment and generate a possibly long three-phase-line (TPL) formed by intersection of the vapor-liquid interface with the heating surface. These properties are also characteristic of the Wei and Honda (2003) structure with its square pin fins.

Schulz et al. (2008) further developed their cylindrical copper pin structure by fabricating the pins with a 45° inclination, see Figure 27. The structures were again fabricated on copper rods and tested in the dielectric liquid "Solkatherm". An average improvement of the heat transfer coefficient of about a factor 2 was reported, in the tested heat flux region of about 0 – 10 W/cm^2. Large incipience hysteresis for the pin fin structure was measured, but not much commented upon.

Forrest et al. (2010) used layer-by-layer deposition of silica nanoparticles to create thin-film coatings on a nickel wire used for pool boiling experiments in de-ionized water. The coatings were 300 to 1000 nm thick depending on how many layers that was applied. The coating dramatically changed the surface wettability of the structures into hydrophilic, superhydrophilic (contact angle <15°) or hydrophobic, but did not change the surface roughness. It was concluded that the nanoporous structure coupled with the chemical constituency of the coatings lead to the enhanced boiling behavior. CHF was enhanced for all types of coating with up to 100% for the superhydrophilic coating. The heat transfer coefficient was only enhanced for the hydrophobic coating with up to 100%, explained by the fact that cavities that are not completely flooded by liquid water can promote bubble nucleation at lower wall superheats. Higher static contact angles (hydrophobic surfaces) lead to higher nucleation site density and thus a higher heat transfer rate for higher contact angle, which is in agreement with previous reports. But, an interesting parameter study and comparison with existing CHF models reveal that the hydrophobic

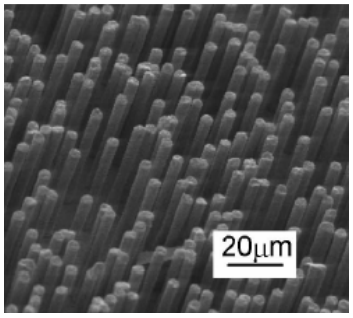

Figure 26. Surface structures consisting of micro pins. (Akapiev et al., 2003)

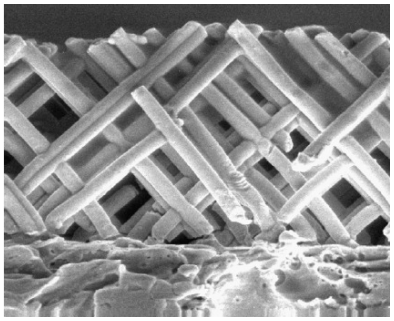

Figure 27. Inclined cylindrical pins of 60μm length and 3μm diameter. (Schulz et al., 2008)

surface has a small receding contact angle, which appears to be the reason for the enhancement of CHF.

Ahn et al. (2006) studied the pool boiling characteristics of vertically aligned multiwalled carbon nanotubes (MWCNT) in PF-5060. The nanotubes were 9 and 25μm in height and 8 to 16 nm in pitch, and were fabricated using CVD on atomically smooth silicon surfaces, see Figure 28. The height of the nanotubes was chosen so that one was smaller and the other was greater than the dynamic value of the estimated minimum vapor film thickness in film boiling (15-20 μm). The 25 μm structure enhanced the heat transfer coefficient slightly more than the 9μm structure, compared to an atomically smooth surface, but the CHF was more enhanced by the 9μm structure. The MWCNT structures serve as enhanced heat transfer surfaces ("nano-fins") which the authors thought could augment the effective area of the heater surface and enhance conduction and convection. The higher thermal conductivity of Carbon Nano-Tubes, 6600 W/(mK) at room temperature can also enhance transient conduction to the liquid phase from the heater surface (during periodic liquid–solid contacts after each vapor bubble departure event). In the nucleate boiling regime – the MWCNT structures disrupt the "thermal micro-layer" region under the bubbles enhancing mixing and thermal transport. The 25μm tall MWCNT structures were thought to disrupt the vapor layer in film boiling causing periodic quenching of the heater.

Chen et al. (2009) reported on the pool boiling heat transfer characteristics of nanowires made out of Si and Cu in deionized water at atmospheric pressure, see Figure 29. The Si nanowires were synthesized by a wafer scale aqueous electroless etching (EE) technique and were 200-300 nm in diameter and about 40-50μm long. The Cu wires were fabricated by electroplating of Cu into nanoscale pores of commercially available porous alumina membranes and were

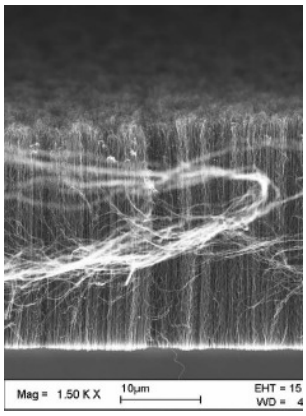

Figure 28. SEM of 25 μm high multiwalled carbon nanotubes. (Ahn et al., 2006)

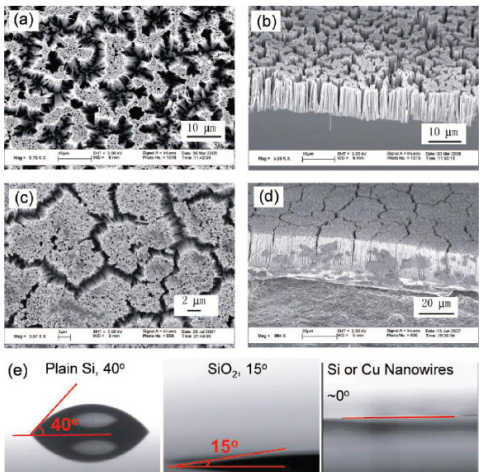

Figure 29. (a) top view of Si Nanowires, (b) cross section of Si Nanowires, (c) top view of Cu Nanowires, (d) cross section of Cu nanowires, (e) static contact angles of a water droplet on surfaces of Si, SiO2, and Si and Cu nanowires. (Chen et al., 2009)

about 200 nm in diameter, 40-50μm long and with a 50% filling ratio. The boiling curves for Si and Cu nanowires are similar, despite the 40 fold difference in thermal conductivity between Cu and EE Si, showing that boiling is dominated by bubble dynamics. CHF and the heat transfer coefficient doubled compared to that of a smooth Si reference surface. The reason for the boiling enhancement is believed to be due to micro-sized defects in the surface structure. The increased surface wettability, with contacts angles close to 0° (superhydrophilic), was believed to be one reason for the enhancements found in CHF, consistent with findings by Forrest et al. (2010)

Ujereh et al. (2007), in a comprehensive study, investigated the saturated pool boiling performance of carbon nano tubes (CNT) on copper and silicone substrates in FC-72. Different area coverage and shapes (islands and grid array) of CNTs were tested, but full coverage was the most effective. CHF was found to be improved by 40% on the fully coated silicone substrate and 5% on fully coated copper substrate. The heat transfer coefficient was improved about 4 times on silicone, but only 30% on copper. Greater enhancement was achieved on silicon than on copper since, compared to uncoated copper surfaces, the uncoated silicon surfaces were very smooth and void of any sizeable nucleation sites to start with. Increasing CNT mesh density on silicon at the nanoscale reduced wall superheat slightly at incipience. However, highly dense CNT arrays also decreased CHF by reducing effective surface area

Phan et. al. (2009) used nanoscale coatings on stainless steel ribbons to modify the topography and chemistry of the surface and thereby varying its static contact angle from 22° to 112° with water, as seen in Figure 30. The coatings were fabricated with various chemical deposition techniques. Unlike surface coatings in the milli- and micro-scale, nanoparticle deposition made it possible to change significantly the surface wettability without a large change of the surface topography. Subcooled boiling experiments, documented with high speed camera, were conducted. For hydrophobic surfaces, bubbles form at low heat flux, but don't detach and therefore coalesce with neighboring bubble sites. Hydrophilic surfaces increase the bubble departure diameter and decrease the bubble emission frequency. For weakly wetted surfaces ($45° < \theta < 90°$), the heat transfer coefficient deteriorates when the contact angle reduces. However, for very wetted surfaces ($\theta < 45°$), the inverse effect was observed: heat transfer coefficient improves with the increase of the wettability.

As has been presented in this chapter, numerous methods and technologies can be employed to produce enhanced surfaces. Different production methods are more or less suitable to different applications and with the aim of enhancing different part of the boiling curve. For instance; the micro pin-fins and channels fabricated with MEMS technology on silicon chips are primarily designed to enhance the CHF in relatively small heat sinks in electronics cooling

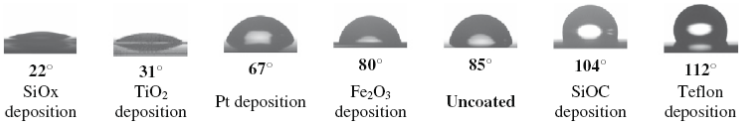

Figure 30. Static contact angles of 2-ll sessile water droplets on stainless steel surfaces with and without nanoparticle deposition. (Phan et. al., 2009)

applications. The same is likely the case for highly structured particle surfaces, such as the 3-D stacks made out of spherical copper particles, even though these might also find its way into nuclear power safety applications.

Machined structured metallic surfaces are typically designed to enhance heat transfer in the fully developed nucleate boiling regime. These types of surfaces are currently widely used in larger industrial applications, such as evaporators in commercial air conditioners. The main drawback of the machined surfaces currently available on the market is that they are difficult to apply to other geometries than tubes.

The most recently reported nano-structures, such as the carbon nano-tubes and nano roughness applied by Launay et al. (2005), Ahn et al. (2006), Ujereh et al. (2007) and Chen et al. (2009) are intriguing in their novelty. It is clear that the chance in nanoscale surface features may change the surface wettability and thereby enhance boiling performance. The potential for nucleate boiling heat transfer enhancement appear to be limited, even though boiling performance of these surface enhancement methods are often compared to that of a microscopically smooth silicon surface, which is a poorly performing surface to begin with. The reviewed publications confirm that the bubble and liquid hydrodynamics and the formation of evaporating thin films is primarily a micro-scale phenomenon and thus the nano-scale enhancement techniques have limited effectiveness. But, it is clear that CHF can be enhanced, which makes these surfaces suitable for small scale, high heat flux applications, such as electronics cooling.

From the review it is also clear that the dominant boiling mechanisms in enhanced structures are inherently different from those of are the smooth and plain surfaces. To augment and alter various boiling mechanisms is obviously the whole purpose of designing an enhanced surface, other than enlarging the effective surface area. Typically in porous structures, such as the classical Nakayama (1980) surface, evaporation through the liquid meniscus formed in corners and thin liquid film dominate two-phase heat transfer. The boiling mechanisms appear to be dominating in porous particle layers such as the surfaces studied by Chang and You (1997). It is also noteworthy that the oscillatory movement of the vapor/liquid interfaces and bubble pumping action all play an important role in the heat transfer.

As seen in the research on for instance the porous wire mesh structures by for instance Li and Peterson (2007) and also the results from the porous honeycomb structure by Mori and Okuyama (2009), the vapor removal mechanism is important for the boiling performance of a certain structure, especially at higher heat flux where the vapor generation rate increases. This poses a challenge to the design of enhanced surfaces, since bubble need to grow sufficiently large inside the structure to form thin liquid films through which effective evaporation can take place, while at the same time, if too large parts of the internal surface dry out when the films have evaporated and before the bubble has been removed then both nucleate boiling and CHF heat transfer performance deteriorates quickly.

Scurlock (1994) found that the general trend for porous particle structures is that thicker structures perform better at lower heat fluxes, but thinner structures

perform better at higher heat fluxes. At higher heat flux, the liquid is pushed out of the porous coating by a vapor blanket and boiling takes place at the surface of the coating and heat transfer is only limited by the thermal conductivity of the porous metal matrix. These results indicate that it would be beneficial to design a surface with vapor escape channels that are gradually increasing with distance from the surface to accommodate larger vapor flow rates at higher heat fluxes. If this was possible, thicker and thus better performing coatings could be used. Franco et al. (2005) showed the advantage of conically shaped vapor escape channels when they were able to further improve CHF by placing finer wire net on the heated surface and larger wire nets on the upper levels, creating conical vapor escape channels.

As will be seen in the next coming chapters, a novel porous surface, easily manufactured on both small and large surfaces of different geometries and with conically shaped vapor escape channels has been developed and tested with some very interesting boiling characteristics.

4 Characteristics of a Novel Dendritic and Micro-Porous Copper Structure

The purpose of the following chapter is to introduce a novel dendritic and micro-porous copper structure that has been developed and tested for enhanced boiling applications. The general manufacturing method, as well as some important fabrication variables and surface characteristics, will be presented. The boiling characteristics and performance of the dendritic and micro-porous surface structure has been the main object of study in all the publications included in this thesis.

A novel surface structure comprising dendritically ordered nano-particles of copper was developed within the scope the thesis research project. Since the micro-porous structure has proven to considerably enhance the boiling performance of a copper surface, patent applications intended to protect the enhancement structure, its fabrication method and its use as a boiling surface, have been submitted to patent authorities in most major markets (initial filing date PRV, 3/3/06, application number: 0600475-8, authors: Furberg, R., Li, S., Mamoun, M., Palm, B., Toprak, M.).

This novel boiling surface may be used in all types of heat exchangers, such as plate heat exchangers, inside or outside tubes in tube-in-shell heat exchanger, hot surfaces in electronics cooling, the evaporating side of heat pipes, refrigeration equipment, air conditioning equipment and heat pumping equipment, thermosyphons, high-efficiency evaporators, in the cooling channels inside water cooled combustion engines and the like.

General fabrication method

Electrodeposition has been recognized, by for instance Xiao et al. (2004), as a suitable process to build and modify three-dimensional structures. Hydrogen evolution during electrodeposition is usually suppressed, since it causes low current efficiency and decreases the density of the deposited metal layer. However, in this work, the hydrogen bubble evolution on the cathode is precisely the process, as first explained by Shin et al.(2003), that leads to the desirable micro-porous structure. The fundamentals of the electrochemical deposition process are illustrated in Figure 31.

To produce the surface of a copper cylinder, later to be used in boiling tests, the polished copper cylinder was used as the cathode and a copper plate functioned as the anode. The two electrode surfaces were fixed parallel in the electrolyte at a certain distance. The electrolyte was a solution of sulphuric acid (H_2SO_4) and various concentrations of copper sulphate ($CuSO_4$). During the deposition a constant DC current was applied, using a precision DC power supply (Thurlby-Thandar TSX3510). The deposition was performed in a stationary electrolyte solution without stirring or N_2 bubbling.

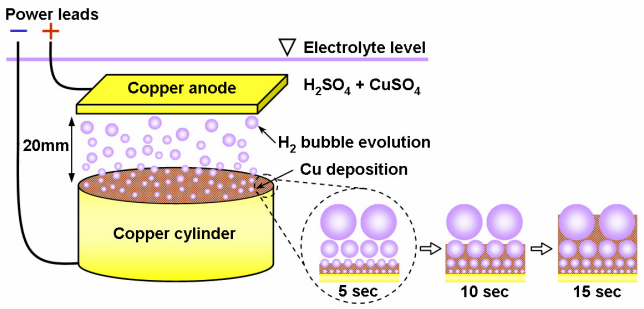

Figure 31. Overview of the electrochemical deposition process.

During the deposition, the growth of the dendritic copper structure is blocked by the hydrogen bubbles, wherefore the hydrogen bubbles function as a dynamic masking template during the deposition. The hydrogen bubbles depart from the surface, rise and merge into larger bubbles, and as a result the pore size of the deposited copper structure increase with distance from the surface, which can be seen from SEM images of structures fabricated with various deposition time.

The deposition process can be described as a competition between hydrogen evolution and coalescence away from the surface and metal deposition on to the surface. At low current density the frequency and nucleation density of the hydrogen bubbles were low, resulting in a dense dendritic structure without any

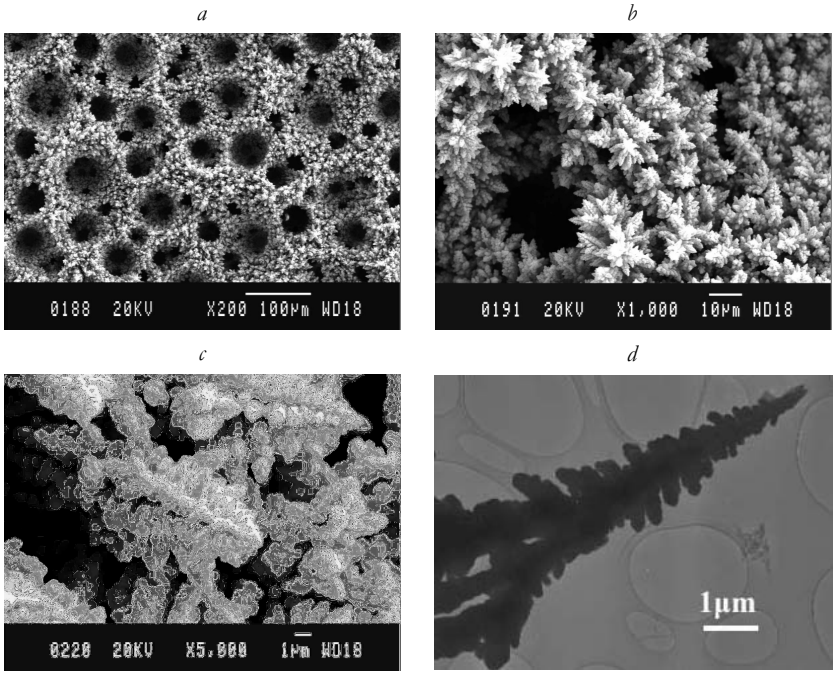

Figure 32. a-c) SEM images of the micro-porous dendritic structures at various magnifications. d) TEM image of part of dendritic branch.

pores, but where only traces of the hydrogen bubble template could be seen at the SEM images. At a current density of about 3A/cm², the bubble population, frequency and coalescence increased to such an extent that the bubbles created permanent voids above the cathode and thereby functioned as a masking template, producing the desired structure.

SEM and TEM images of the micro-porous structure and the dendritic sub-structure are shown in Figure 32. Detailed analysis of the dendritic branches showed that the branches comprise nano-sized grains between 10-20 nm.

Important Fabrication Variables

The features and properties of the micro-porous surface structure with dendritically ordered nano-particles can be controlled and altered, both on a macro, micro and sub-micron level, by employing various fabrication techniques and altering certain manufacturing parameters. This makes it possible to produce an optimized structure for a specific application.

Annealing

The usefulness of the structure in real heat transfer applications would be limited, since the structural stability of the micro-porous surface structure is relatively weak. For this reason, the structure was subjected to an annealing process. Annealing is a heat treatment process which takes place below the melting temperature of the copper and under a reducing atmosphere (hydrogen) to avoid oxidization of the copper. After the annealing treatment, the micro-porous structure remained intact (pore size, thickness of the structure, pore density), but the sub-micron related features of the structure changed, due to the growth of the grain size of the nano-dendritic branch-like features, which can be visually verified in Figure 33. As the grains grew during annealing treatment, the interconnectivity of the grains was also improved, and the grain boundary effect of nanoparticles was reduced.

The annealing treatment resulted in improved mechanical stability of the structure and increased electrical-, and therefore also thermal-, conductivity of the structure. The annealing improved boiling heat transfer performance compared to the non-annealed structure, which will be expounded upon in the next chapter.

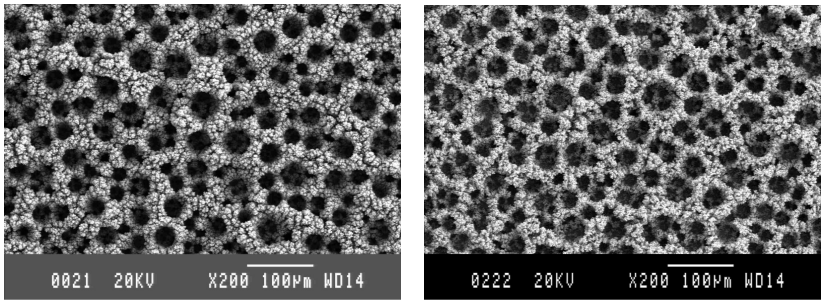

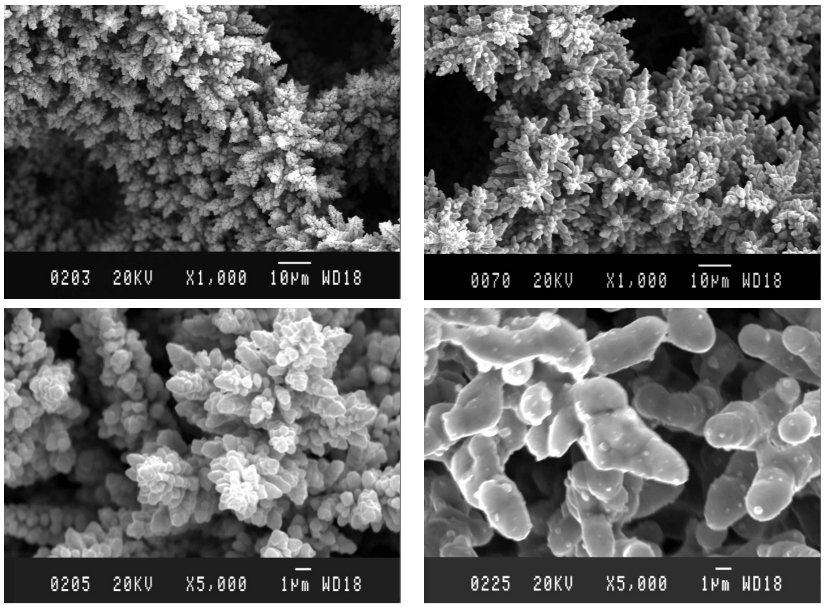

Figure 33. Dendritic structure before (left side) and after (right side) annealing. x200 (top), x1000(middle), and x5000 (bottom) magnification.

Time and Concentration

Three important manufacturing parameters during the electrodeposition process are deposition time, current density and molar concentrations of sulphuric acid and copper sulphate. In summary, longer deposition time and higher molar concentration result in a thicker structure with larger pores. The pore size was measured at the top of the structure, which are the pores seen from SEM images. As illustrated in Figure 34, thickness, pore size and deposition amount are almost linear functions of the deposition time.

Surface Orientation and Geometry

The orientation of the cathode was also affecting the dynamics of the hydrogen evolution and the Cu deposition. With the cathode oriented vertically (90°) the result was almost identical to that of a horizontal orientation (0°). But, with the cathode facing down the hydrogen bubbles would not easily escape, but rather coalescence and eventually form a large bubble covering the whole surface. Hence, the Cu deposition was completely obstructed after approximately 25 sec. of deposition. The structure was similar to the ones made at 0° and 90°, but since the growth only continued for 25 sec. there was a limit to the thickness of the structure. Furthermore, since the bubbles coalesced and stayed on the surface at 180° deposition, less current density was needed to create the porous structure. Since the structure may be fabricated on a surface of any direction, it is possible to apply the micro-porous enhancement structure to many different geometries that might be interesting heat transfer applications, such as plate heat exchangers, inside and outside of tubes, fins, etc.

Additives

The pore sizes and wall structures could be altered by using various additives in the electrolyte. One such additive, among many others, is hydrochloric acid (HCl), which had the effect of considerably reducing the elementary branches in the structure and changing the shape of the pores, see Figure 35.

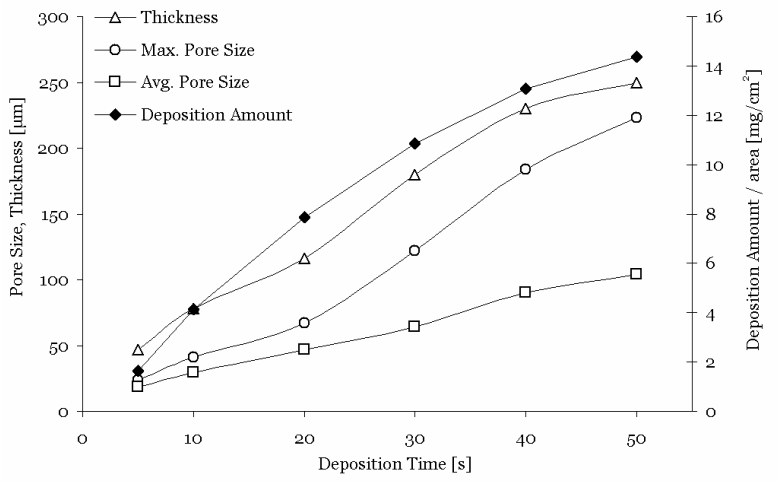

Figure 34. Various characteristics of the micro-porous structure as a function of time at 1.5M H_2SO_4 and 0.4M $CuSO_4$, and a current density of 3A/cm.

Temperature and Pressure of Electrolyte

By increasing the temperature of the electrolyte, the pore size of the structure was increased considerably. The dendritically formed grains were similar in size. The deposited amount was also found to increase. By enclosing the electrodeposition set-up in a pressure vessel, it was possible to fabricate the structure under varying pressures. At low pressure 50 mbar (abs), the pore size was found to be reduced, which was unexpected considering that gas bubbles expand as under lower pressure. It was also observed that the micro-porous structure at low pressures was more homogeneous than at higher pressures. At higher pressure, 3.0 bar (abs), the change in pore size was negligible compared to deposition at atmospheric conditions.

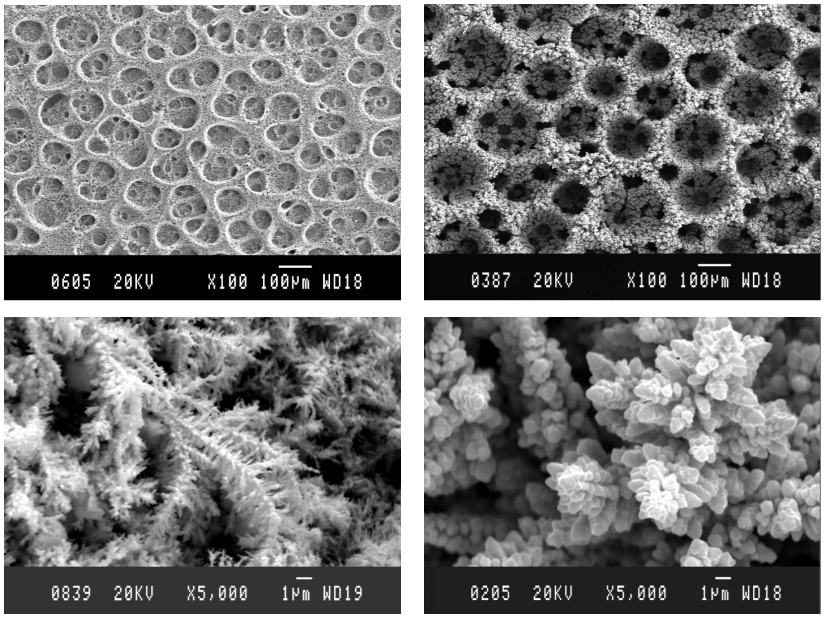

Figure 35. (left side) Micro-porous structure fabricated with 50mM HCl additive (right side) Structure fabricated without additives.

Electrical and Thermal Conductivity of Structure

The annealing treatment is one way to increase the connectivity of the grains. Due to the complication associated with directly measuring the thermal conductivity of a thin porous structure such as the nano-dendritic micro-porous structure, a simple indirect method was developed where the electrical conductivity of the structure was measured, before and after annealing.

Since the electrical conductivity is proportional to the thermal conductivity of a metal, according to the Wiedemann-Franz law, this method ought to give an indication of how the thermal conductivity of the structure, λ, is changed after the annealing treatment. Since the electrical conductivity is inversely proportional to the electrical resistance, R, the relationship is:

$$\frac{\lambda_{\text{annealed}}}{\lambda_{\text{non-annealed}}} = \frac{R_{\text{non-annealed}}}{R_{\text{annealed}}}$$

To estimate the thermal resistance in the dendritic and micro-porous structure, a test structure was first fabricated in-between two thin copper plates, which had been electrically insulated and fixed with a ceramic insulation paste, see Figure 36. One plate functioned as anode and one as cathode and during the electrodeposition step, the structure grew until it connected to the anode, resulting in electric short circuiting of the two plates and a rapidly increasing current. The fabrication conditions were 1.5M H_2SO_4 and 0.4M $CuSO_4$ and a current density of 3A/cm. The electrical resistance between the two plates was measured to 0.23Ω.

Then the entire test object was subjected to a 5 hour and 500°C annealing treatment. After annealing, the electrical resistance between the two plates was measured to 0.01Ω. Hence, the annealing treatment decreased the electrical resistance 20 times, which indicates an increase of thermal conductivity of the annealed structure compared to the non-annealed.

A major uncertainty of this test is the possible existence of a large electrical connection resistance between the structure and the anode. If this is the case, it is possible that the annealing treatment substantially lowers this electrical

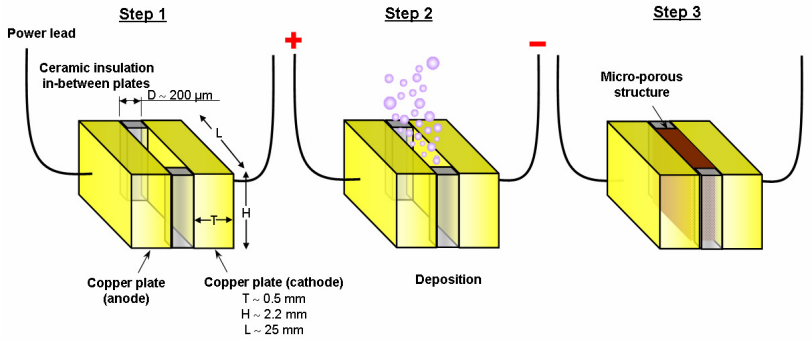

Figure 36. Fabrication of micro-porous structure in narrow gap.

connection resistance and hence the reduction in total electrical resistance would not be due to a reduction of the resistance through the structure.

Tests of the mechanical stability of the structure were presented in the licentiate thesis, Furberg 2006, and will not be expounded upon much here. But, it must be mentioned that the mechanical stability of the structure is of utmost importance for the possible usage of the surface.

Conclusions

The simplicity of the described manufacturing method, the possibility to vary the characteristics of the porous layer and different geometries to which the surface structure could be fabricated are all important factors that makes the structure an interesting candidate for enhance boiling applications. In the following chapters, the results and analysis will be presented from the boiling performance of different variants of the structure, such as annealed and non-annealed, different layer thickness, etc.

5 Nanostructured and Micro-porous surface in Pool Boiling

As seen in appendices I - III, the nano- and micro-porous copper structure was studied quite extensively in various pool boiling experiments. Different parameters, such as; thickness of the porous layer, presence of vapor escape channels, annealed or non-annealed structure, and different boiling fluids were investigated. Some of the tests were filmed with a high speed camera from which visual observation were made, as well as quantitative bubble data extracted. A brief overview of the findings and conclusions will be presented here. Finally, an attempt has been made to synthesize the findings in a boiling model for the enhanced surface, which has not been included in any of the attached publications.

Pool boiling experiments in R134a at saturated conditions were conducted at 4 bar absolute pressure (corresponding to 8.9°C). The micro-porous surface was fabricated on one end of a 6 mm thick copper cylinder with a diameter of 15 mm. After the application of a wire heater, the copper cylinder and was inserted into a teflon insulation casing.

As seen in Figure 37 a and b, the boiling performance of the enhanced surfaces was found to be dependent on the thickness of the structure, the interconnectivity of the grains in the dendritic branches and the presence of vapor escape channels (each curve represents a different layer thickness, where

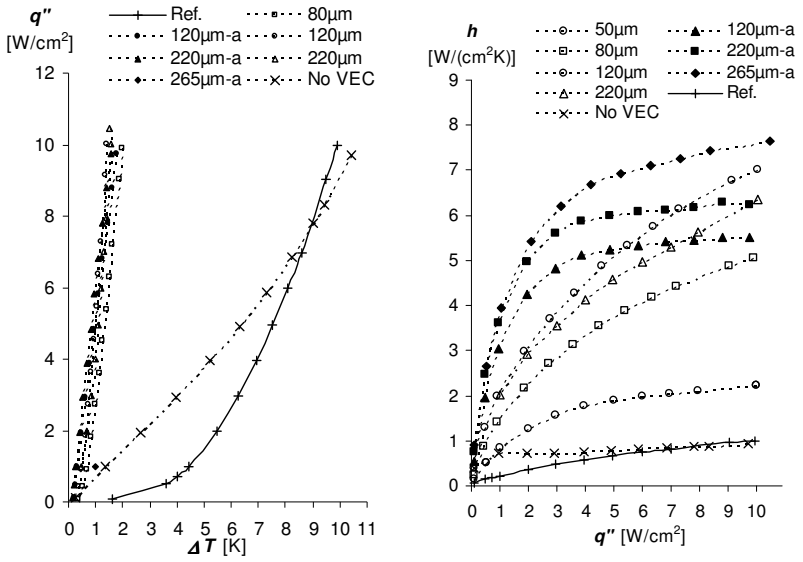

Figure 37. a. Temperature difference vs. heat flux for several enhanced surfaces and a reference copper surface.

b. Heat transfer coefficient vs. heat flux for the same surfaces as in a.

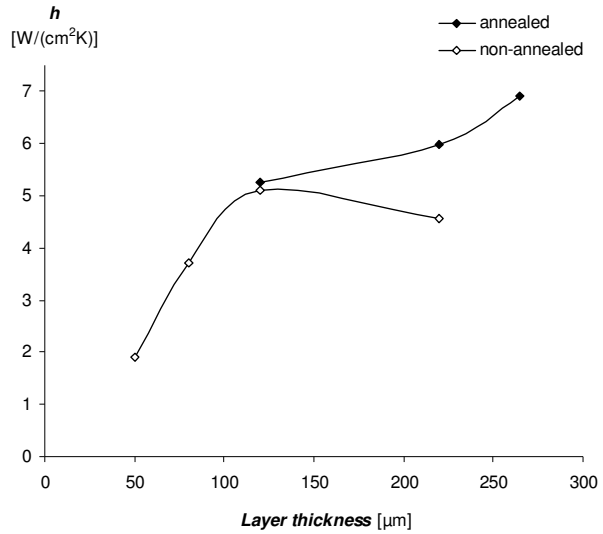

Figure 38. Heat transfer coefficient vs. layer thickness at 5 W/cm² for annealed and non annealed surfaces

the label "-a" after the layer thickness denotes that the surface has been annealed. "No VEC" stands for no vapor escape channels and "Ref." for a plain copper reference surface). All of the enhanced surfaces sustained nucleate boiling at lower surface superheat than the reference surface. Enhancement ratios of an order of magnitude may be seen compared to the reference surface.

As seen in both Figure 37 and Figure 38, the heat transfer coefficient was a strong positive function of the layer thickness. The performance of the annealed surface increased with layer thickness all the way up to the thickest layer tested. The performance of the non-annealed surface improved with increased thickness up to 120µm, after which the heat transfer coefficient started to level off, or deteriorate.

Figure 37 reveals that the 120µm-a and 220µm-a annealed surfaces had a higher heat transfer coefficient than their non-annealed counterparts up to about 6 W/cm², above which the non-annealed surfaces performed slightly better. As seen in previous chapter, the annealing treatment improved the grain connectivity and can therefore be expected to increase the thermal conductivity of the structure with up to 20 times. The increase in thermal conductivity was particularly important for the heat transfer mechanism at low heat flux, but not in the high heat flux range, a behavior also found by Li and Peterson (2007) when experimenting with porous surfaces fabricated out of sintered copper wire mesh. Li and Peterson (2007) suggested that boiling initially occurs on the heated wall and then progresses through the solid structure for the porous coating once the superheat reaches a level that is directly related to the heat flux. Another explanation to this behavior could be the hydrodynamics involved in the liquid supply to the structure starts to limit heat transfer at higher heat flux and thus the thermal conductivity of the structure is of less importance.

The interesting resemblance between the manufacturing process of the structure and the boiling phenomena itself is remarkable. The vertical channels formed by the electrodeposition process with the template of hydrogen evolution have a geometrical form that is well-suited for vapor transportation, since the tunnel diameter is increasing with distance from the substrate surface, leaving enough space for the growing bubble. The hydrogen bubbles, which are departing during the electrodeposition, seek the lowest resistance path and therefore facilitate the formation of low impedance vapor escape channels. The boiling performance of the dendritic structure without any vapor escape channels ("No VEC" in Figure 37) confirmed that the vapor escape channels are essential to effective bubble transport from the structure, especially at higher heat flux where more vapor is formed. The performance was similar to the other enhanced surfaces at the lowest heat flux, but the heat transfer coefficient is fairly constant at about 0.7 W/(cm²K) for all heat flux.

The initial analysis of the pool boiling results suggested that combination of suitable vapor escape channels; high layer porosity, dendritic branch formation and large surface area were features of the nano- and micro-porous copper structure that contributed to the boiling enhancement.

In an effort to further the understanding of the heat transfer mechanisms in the structure, a high speed visualization system was set up, as seen in appendix III. Data on bubble size, bubble frequency density, heat transfer coefficient and the latent and sensible heat flux contributions were collected and calculated at heat fluxes varying between 2 and 15 W/cm². Both R134a and FC-72 were used as fluids under saturated conditions, 5 and 1 bar respectively (corresponding to 15.7°C and 55.9°C respectively). The annealed surface structure was 250µm thick with an average top layer diameter of 105µm and a top pore density of about 30/mm². The reference surface was a plain copper surface, polished with 320p emery paper.

Two different type of high speed videos were obtained, as illustrated in Figure

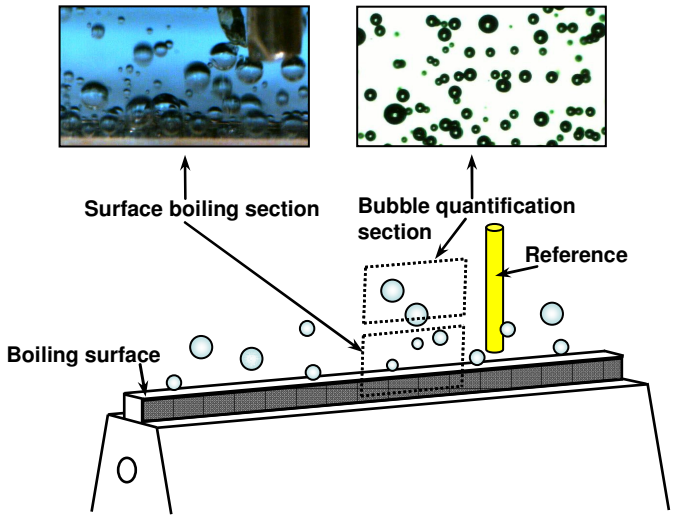

Figure 39. Filmed sections during high speed visualization experiments.

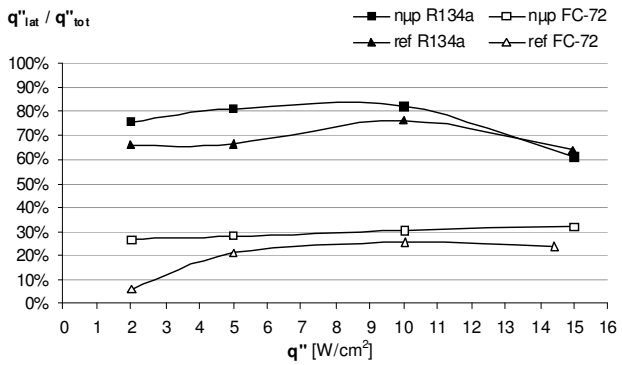

Figure 40. Latent heat flux contribution for both plain and enhanced surfaces in FC-72 and R134a.

39: a bubble quantification section and a surface boiling section. The bubble quantification section was a back-lit area located 1 mm above the boiling surface to avoid the influence of the intense bubble coalescence at the surface and thereby be able to measure the bubble size and velocity. The surface boiling section was front-lit to give a more qualitative close up view of the bubble growth, departure and merger taking place on the porous structure.

The enhanced surface produced smaller bubbles and sustained a high bubble frequency density in both fluids, even at low heat flux. From the measured bubble diameters and frequencies, the latent heat flux contribution was calculated, with the results shown in Figure 40. The difference in latent heat flux between the two fluids is due to the difference in thermodynamic properties. This difference is captured quite well by the Jacob number defined as the ratio of sensible to latent heat, according to:

$$Ja = \frac{\rho_{liq.} c_p \Delta T}{\rho_{vap.} h_{fg}} \qquad (1)$$

where ΔT is the overall temperature difference that was measured between the surface and the saturated liquid, c_p is the liquid specific heat, ρ_{liq} and ρ_{vap} is the density of the liquid and vapor respectively and h_{fg} is the enthalpy of vaporization. The Jacob number is only between 0.1 and 0.5 for the enhanced surface in R134a while it is between 4 and 8 for FC-72. Hence, there is more than an order of magnitude difference, primarily due to the higher enthalpy of vaporization for R134a (186 kJ/kg, compared to 87 kJ/kg for FC-72) and the 5 times higher pressure used for the R134a tests, which results in a 3.5 times smaller liquid to vapor ratio than for FC-72.

By measuring the bubble size and frequency as close as possible to the boiling surface, the relation between latent and sensible heat gives information regarding the heat transfer mechanisms inside, or immediately outside, the porous layer. Above the window in which measurements were taken, the sensible heat, which resulted in slightly superheated liquid, must have either been; transferred to the bubbles through evaporation over the bubble / liquid interface as the bubbles travelled up toward the free liquid surface, or undergone

the phase change through evaporation at the free liquid surface located 5 cm above the boiling surface.

To analyze the data further, a superposition model was suggested where:

$$q''_{tot} = q''_{lat} + q''_{sens} \quad (2)$$

which could also be expressed as;

$$h = h_{lat} + h_{sens} \quad (3)$$

The heat transfer coefficient for the enhanced surface could thus be expressed as;

$$h_{n\mu p} = h_{lat\_n\mu p} + h_{sens\_n\mu p} \quad (4)$$

and the heat transfer coefficient for the reference surface as;

$$h_{ref} = h_{lat\_ref} + h_{sens\_ref} \quad (5)$$

Since all parameters in (2) are determined from the experiments (q''_{tot} from input power and q''_{lat} from bubble size and speed measurements) the heat transfer coefficients for latent and sensible heat respectively, in equations (4) and (5), could be calculated according to the general form of:

$$h_{lat} = \frac{q''_{lat}}{\Delta T} \quad (6)$$

and

$$h_{sens} = \frac{q''_{sens}}{\Delta T} \quad (7)$$

where ΔT is the overall temperature difference that was measured between the surface and the saturated liquid. The calculated latent and sensible heat transfer coefficients for the micro-porous surface are presented in Figure 41. The heat transfer in R134a is clearly dominated by latent heat transfer while the opposite is the case for FC-72. These results correlate quite well with the Jacob number in equation (1) in that the ratio between sensible to latent heat transfer coefficients is about an order of magnitude larger for FC-72 compared to R134a.

The latent and sensible heat transfer coefficients for the plain surface were also calculated, according to equations (6) and (7). As a way to compare the latent and sensible heat transfer coefficients for the micro-porous surface and the plain reference surface, enhancement factors, *L* and *S*, were introduced and calculated according to:

$$L = \frac{h_{lat\_n\mu p}}{h_{lat\_ref}} \quad (8)$$

and

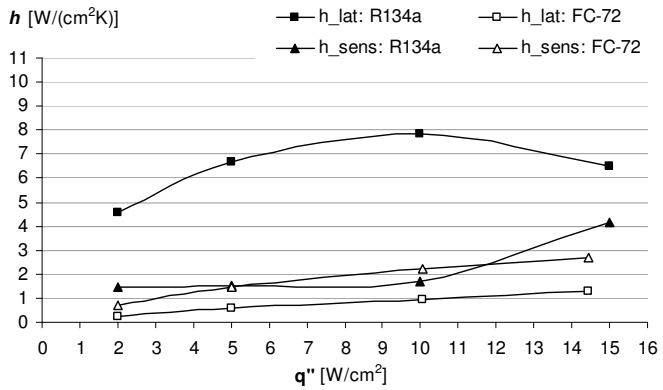

Figure 41. Latent and sensible heat transfer coefficients vs. heat flux for the micro-porous surface in R134a and FC-72.

$$S = \frac{h_{sens\_n\mu p}}{h_{sens\_ref}} \qquad (9)$$

The calculated enhancement factors are presented in Figure 42. The two-phase heat transfer mechanism was enhanced 4 to 10 times by the porous structure, as seen in the *L* factor. At most conditions and for both fluids, the L factor is larger than the S factor, indicating that the enhancement of the latent heat transfer mechanism was the main reason for the increase in overall heat transfer coefficient. The high nucleation site density, even at low temperature differences, is one factor explaining the large *L* multiplier. It is likely that the two-phase heat transfer mechanisms are changed in the enhanced surface. The large internal surface area of the dendritically shaped structure may facilitate highly effective evaporation of thin liquid films inside the porous structure, or along triple phase lines close to the bottom of the surface.

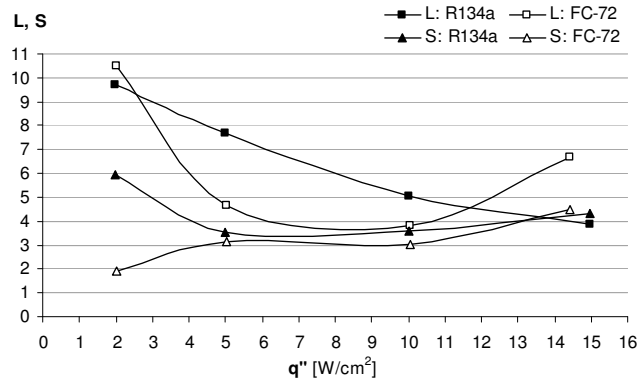

Figure 42. Latent (L) and sensible (S) enhancement factors for the micro-porous surface compared to a plain reference surface in R134a and FC-72.

Other than augmenting the bubble formation, growth and departure, the porous structure also notably enhanced the heat transfer mechanisms of sensible heat transfer by 2 to 6 times, as seen in the *S* factor in Figure 42. The enhanced single-phase convection heat transfer may be due to the strong convection caused by the agitation of the vapor bubbles inside, and immediately outside, the porous layer and by the increase in the number of nucleate sites. Furthermore, the copper enhancement structure itself could act as an extended surface as the liquid is moving through the highly porous walls. At higher heat fluxes, and thus higher temperature differences, the enhanced single-phase convection effect caused by the micro-porous structure increases and the difference between the L and S factors are smaller.

Conclusions

The pool boiling experiments have shown that the dendritic and micro-porous surface structure is very effective in enhancing boiling heat transfer. Various surface structure variables, such as layer thickness and the interconnectivity of the grain (annealing treatment) impact the boiling performance of the surface. Visualization results show that this enhancement mechanism is due to both single- and two-phase heat transfer within the porous structure. The presence of suitable vapor escape channels and the large internal surface area are thought to be important surface features.

The experimental data obtained in these various pool boiling test, appendices I – III, do not fully reveal the exact nature of the heat transfer mechanisms inside the porous structure. They indicate But, it is possible, given the data obtained and the conclusions that have been drawn from it, to initiate a discussion around a mechanistic boiling model. This model will be presented in the next chapter.

6 Boiling Model for Dendritic and Micro-Porous Structure

The model presented in this section has not been published elsewhere and is therefore not included in any of the attached publications.

In general, energy is transferred from a boiling surface either as latent heat in the departing bubbles, or as sensible heat in the superheated liquid rising from the surface. In enhanced boiling; evaporation and convection to the liquid can occur both on the *exterior* of an enhanced boiling surface, as for conventional boiling as seen in Figure 2, or in the *interior* of the passageways of the structure. Thus, as pointed out by Thome (1990), there are basically four different ways in which heat can leave an enhanced boiling surface:

- in bubbles formed within the enhancement structure;
- in bubbles growing on the exterior surface. Bubbles that originated either on the exterior, or the interior of the surface;
- in liquid that has been superheated from having been pumped into and out of the enhancement structure by the pumping action induced by growing and departing bubbles;
- in liquid that has been superheated from having flowed over the exterior surface.

Based on the conclusions and insight made from pool boiling test attached in appendices I – III, following hypothesis is suggested for the dominant boiling mechanisms in the dendritic and micro-porous structure: *The main two-phase heat transfer mechanism inside the porous structure is micro-layer evaporation formed by an oscillating vapor-liquid front with low resistance vapor transport through the vapor escape*

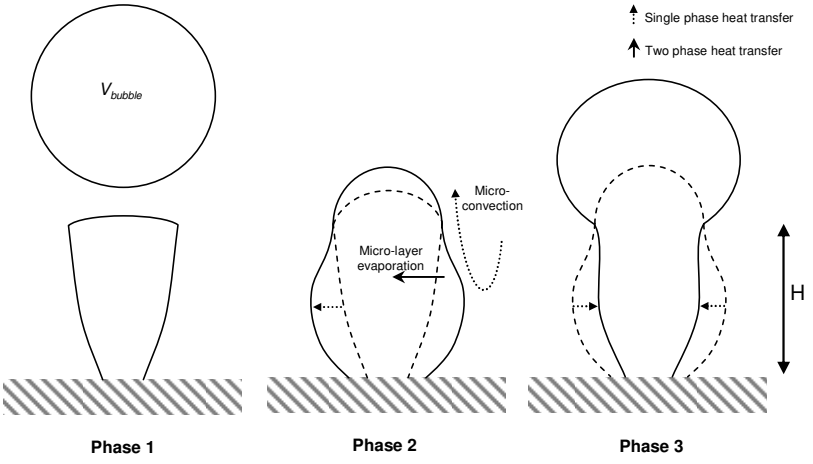

Figure 43. Different phases during the boiling cycle.

channels. The single-phase heat transfer mechanism, where superheated liquid is pumped out of the structure, is liquid motion induced by the bubble pumping action and the oscillating vapor front.

Hence, the main single- and two-phase heat transfer mechanisms for the micro-porous surface are thought to take place inside the structure. Figure 43 illustrates schematically an overview of the boiling process in the porous structure, which bears some marks of similarity with the dynamic liquid suction-evaporation model first presented by Nakayama et al (1982).

Phase 0: After boiling incipience, the porous structure contains vapor patches which eliminate the need for bubble nucleation from microscopically small vapor nuclei.

Phase 1: After bubble necking and departure, a vapor volume is left inside the porous structure with a large bubble radius which, due to low surface tension forces, balances a low vapor pressure inside the vapor volume. Visual observation from high speed filming has shown that the bubble dome may be located at the perimeter of the top pore or one level down in the vapor escape channel.

Phase 2: As the vapor volume increases, the radius of the bubble dome decreases to a minimum at the pore opening, resulting in increasing vapor pressure inside the bubble. Due to the pressure increase, the vapor front advances into the porous walls of the structure. Thin liquid films remain on the dendritic branches behind the advancing vapor front, due to surface tension and adhesion and friction forces. Large vapor/liquid interfacial area and the low thermal resistance over the thin liquid films facilitate high evaporation rates and latent two-phase heat transfer: micro-layer evaporation. The advancing vapor front and the departing bubbles also induce liquid convection inside the porous structure where the large internal surface facilitate single-phase heat transfer into liquid that is being superheated and eventually pumped out of the structure. Some heat is certainly also being transferred over the bubble dome over the vapor/liquid interface inside the structure.

Phase 3: Liquid inertia inside the structure and the bubble buoyancy force will eventually result in an increase in the bubble dome radius, thus lowering the vapor pressure inside the bubble. Vapor will now flow back into the rising bubble dome through the vapor escape channel and the bubble necking and departure process begins. Liquid rewets the parts of the dendritic structure from which evaporation have taken place.

As in the superposition model presented in section 5, the heat transfer coefficients for single- and two-phase flow are added to account for the total heat transfer coefficient. In the remaining part of this section, these heat transfer mechanisms and the resulting single and two-phase heat flux for the boiling tests presented in appendix III in R134a will be analyzed and modeled.

Two-phase Heat Transfer

Phases 1-3 of the boiling process are in rapid succession, which leads to an oscillating vapor/liquid interface within the structure. Consider the heat flow that is transported from the substrate, conducted through the dendritic branches and through the thin liquid film on the surface of the branches. With the

assumptions that the vapor escape channel is left filled with vapor after a departing bubble and that all the vapor is generated through thin film evaporation inside the porous structure, the bubble volume, V_{bubble} of the departed bubble must have been produced inside the porous structure corresponding to the evaporation of a liquid volume, V_{liq_evap}, according to:

$$V_{liq\_evap} = V_{bubble} \cdot \frac{\rho_{vap}}{\rho_{liq}} \qquad (10)$$

As the vapor volume increases and the vapor front advances an average distance of, ΔR_{vap} , into the porous structure, the heat transfer area, A_{ht} , is the surface area of the dendritic structure that is covered in a liquid film of an average thickness, δ_{film}, as seen in Figure 44.

The heat transferred through the liquid film, as calculated per vapor escape channel (or pore), *P*, is governed by conduction, as seen in:

$$\frac{Q'_{lat}}{P} = \frac{\lambda_{liq} \cdot A_{ht}/2 \cdot \Delta T_{film} / \delta_{film}}{P} \qquad (11)$$

$Q'lat$ is latent heat flow rate, λ_{liq} is the thermal conductivity of the liquid and ΔT_{film} is the temperature drop over the liquid film. Since the vapor front is assumed to oscillate with the bubble departure frequency a certain distance into the structure, the time averaged heat transfer area through which thin film evaporation occurs can be approximated with $A_{ht}/2$.

If the ratio between active pores and total number of pores is denoted, η , the heat transfer area per pore may be calculated as:

$$\frac{A_{ht}}{P} = \frac{A_{ht}}{B} \cdot \frac{B}{P} = \frac{A_{ht}}{B} \cdot \eta \qquad (12)$$

η was estimated from the high speed videos of the surface to be 1, even at the lowest heat flux. In other words, all pores were active at all heat fluxes. The latent heat transfer per projected top area:

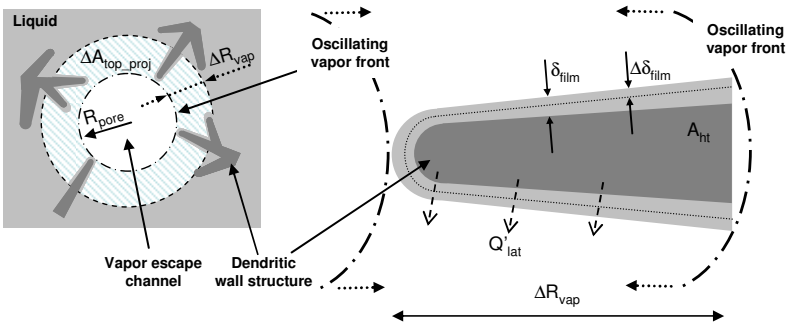

Figure 44. A detailed view of the thin film evaporation on the dendritic structure.

$$q''_{lat} = \frac{Q'_{lat}}{A_{top\_proj}} \qquad (13)$$

was calculated from bubble data, as described in appendix III. The pore density, P_ρ, defined as the number of pores, P, per projected top area, was calculated from SEM pictures to 30/mm^2 and is expressed as:

$$P_\rho = \frac{P}{A_{top\_proj}} \qquad (14)$$

Hence,

$$\frac{Q'_{lat}}{P} = \frac{q''_{lat}}{P_\rho} \qquad (15)$$

and the total heat flux may be derived from equations (11) to (15) to:

$$q''_{lat} = P_\rho \cdot \frac{\lambda_{liq} \cdot \Delta T_{film}}{\delta_{film}} \cdot \frac{A_{ht}}{2B} \cdot \eta \qquad (16)$$

Consider a vapor volume that has a cylindrical shape around the vertical central axis of the vapor escape channel and is extending top to bottom through the porous layer. The bubble volume, V_{bubble}, may be calculated from:

$$V_{bubble} = \Delta A_{top\_proj} \cdot H \cdot \phi - A_{ht} \cdot \delta_{film} \qquad (17)$$

where H is the height of the porous layer and ΔA_{top_proj} is the change in the top projected area of the vapor volume inside the porous layer as seen in Figure 44. ϕ is the porosity of the porous structure (93%). The evaporated liquid volume is proportional to the change in liquid film, $\Delta\delta_{film}$, and may be approximated with:

$$V_{liq\_evap} = A_{ht} \cdot \Delta\delta_{film} \qquad (18)$$

Surface gas adsorption measurements were conducted to estimate the surface area of the structure. Assuming the particles to be monodispersed and spherical with a size of 1.74 μm, the surface area of the annealed porous structure was measured with BET surface area measurements to 0.38 m^2/(g of wall structure), which for a 250μm thick structure corresponds to 57 m^2 of wall structure/m^2 of top projected wall structure. 57 m^2 of wall structure/m^2 agrees well with calculations of the surface area based on geometrical dimensions obtained from SEM pictures. As general definition, the area enlargement factor, f_{area}, may thus be defined as:

$$f_{area} = \frac{A_{structure}}{A_{top\_proj\_wall}} \qquad (19)$$

where $A_{top\_proj\_wall}$, is the area of the top projected wall structure. Applying equation (19) to the area around a pore, the change in $A_{top\_proj\_wall}$ due to the expanding vapor volume inside the structure corresponds to ΔA_{top_proj}, in equation (17) and Figure 44, which means that $A_{structure}$ is the surface area of the

porous layer that is swept by the advancing vapor front, equivalent to A_{ht}. Therefore, equation (19) may be expressed as:

$$f_{area} = \frac{A_{ht}}{\Delta A_{top\_proj}} \qquad (20)$$

The dendritic branches could be seen as extended surfaces, or fins, since heat is transferred from the surface substrate and through the dendritic branches and finally through the thin liquid film. The temperature difference needed to transport the heat through the branch structure is not negligible and can be taken into account using the fin efficiency concept. Fin efficiency, η_{fin}, is defined as:

$$\eta_{fin} = \frac{Q'_{fin}}{Q'_{max}} \qquad (21)$$

where Q'_{fin} is the actual heat transferred through the fin and Q'_{max} is maximum heat dissipated through the fin, if the entire fin were at the base temperature proportional to the temperature difference between bulk fluid and the base of heater, ΔT, which was measured in the experiments. Since Q'_{fin} is the heat that is transferred through the fin, it is proportional to the temperature difference across the thin liquid film, ΔT_{film}. Thus, the fin efficiency could be defined as:

$$\eta_{fin} = \frac{\Delta T_{film}}{\Delta T} \qquad (22)$$

Assuming that shape of the dendritic branch can be approximated with that of a pin fin, the fin efficiency may be calculated from well known correlations found in literature such as Incropera and DeWitt (2002) according to:

$$L_c = L + D/4 \qquad (23)$$

$$m = \sqrt{\frac{4h_{ht,fin}}{\lambda_{fin} D_{fin}}} \qquad (24)$$

$$\eta_{fin} = \frac{\tanh mL_{fin}}{mL_{fin}} \qquad (25)$$

where D_{fin} is the diameter of the fin which could be estimated from SEM pictures of the structure to about 1 μm. The fin length, L_{fin}, , is difficult to measure from the available SEM images. The shape of the dendritic branch structures from the substrate to the end tip of the branch resembles that of a fractal line. Using the Koch snowflake fractal geometry and estimating that each branch segment is about 30μm long, the total fin length may be calculated to 2.7 mm. λ_{fin} is the thermal conductivity of the fin, which for the annealed structure can be assumed to be the same as copper, 400 W/(mK). $h_{ht,fin}$ is the

heat transfer coefficient on the surface of the fin, which may be estimated from conduction through the thin liquid film:

$$h_{ht,fin} = \frac{\lambda_{liq}}{\delta_{film}} \qquad (26)$$

The heat transfer area per pore, A_{ht}/P, is calculated from equation (12). Equations (16) and (22) thus gives:

$$q''_{lat} = P_{\rho} \cdot \frac{\lambda_{liq} \cdot \Delta T \cdot \eta_{fin}}{\delta_{film}} \cdot \frac{A_{ht}}{2B} \cdot \eta \qquad (27)$$

where q''_{lat} is the latent heat flux. With $\eta = 1$, equation (27) can also be expressed, using equations (17) and (20), as:

$$q''_{lat} = P_{\rho} \frac{\pi}{12} \cdot \frac{\lambda_{liq} \Delta T \eta_{fin} D_{dep}^{\ 3}}{\delta_{film} H \phi \big/ f_{area} - \delta_{film}^2} \qquad (28)$$

where D_{dep} is the bubble departure diameter before possible coalescence with another bubble. Except for the liquid film thickness, δ_{film}, , all variables in equation (28) are either measured, calculated or estimated from experiments and SEM pictures of the structure.

As described in detail in appendix III, the bubble departure diameter was measured 1 mm above the surface. Thus, the bubble departure diameter measured at higher heat flux was found to be that of already merged bubbles. Surface videos reveal that bubbles merger occurs already at 2 W/cm^2. Using high speed pictures of the pore openings, the surface boiling section, as seen in Figure 39, the bubble diameters before merger were estimated for R134a. Bubble departure measurements were not obtained for FC-72 since vivid bubble merger at the surface made it difficult to estimate the vapor volume generated from one pore.

Figure 45 shows the average calculated thickness of the liquid film, δ_{film}, , during bubble cycle as a function of total heat flux. At different heat flux in R134a, the liquid film thickness was calculated to be just below 4 μm for all heat flux. The necessary change in liquid film thickness, $\Delta\delta_{film}$, was calculated from equations (10) and (18) to only a small fraction of the liquid film thickness, δ_{film}.

No experimentally validated correlations have been found with which to calculate the thickness of a liquid film formed under an advancing vapor front inside such small diameter flow paths as those within the porous structure. But, correlations suggested by Han and Shikazono (2010), where the liquid film thickness under an advancing vapor fronts in micro tubes was measured, indicate that with the low velocity with which the vapor advances inside the porous structure (calculated to about 19-37 mm/s), films with thicknesses even below 0.1 μm may form. Considering that the characteristic geometrical dimensions of the dendritic structures are in the 1-10μm range and that the

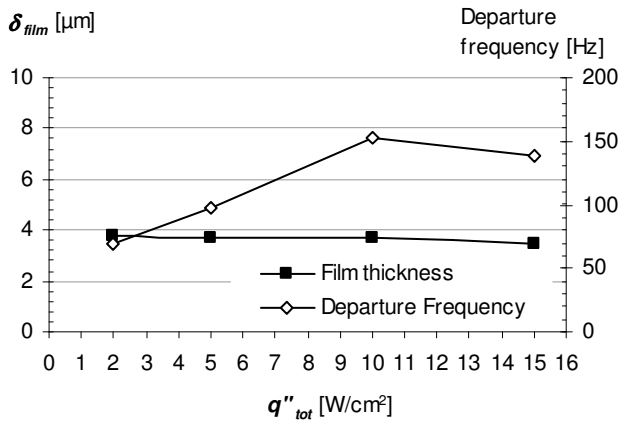

Figure 45. Average thickness of thin film, δ_{film}, during bubble cycle and the bubble departure frequency, as a function of total heat flux.

velocity of the advancing vapor front is low, the calculated film thickness appears to be in the right order of magnitude.

The calculated change in film thickness is rather constant. As seen in equation (28), the calculated liquid film thickness is highly sensitive to the estimated bubble departure diameter.

The bubble departure frequency per pore, f_{Hz}/P, was calculated as:

$$\frac{f_{Hz}}{P} = \frac{q''_{lat}/P}{V_{bubble} \cdot \Delta h_{fg} \cdot \rho_{vap}} \qquad (29)$$

Figure 45 also shows the calculated bubble departure frequency to be in the 50-150 Hz range; frequencies that are in a range that could be expected, see for instance Kim and Kim (2006).

Equation (28) is obviously not a correlation with which the latent heat transfer could be calculated from known surface and liquid properties, since the thickness of the liquid film, δ_{film}, , and the bubble departure diameter, are both unknown. Accurate prediction of bubble departure diameter in pool boiling is notoriously difficult, primarily due to unknown contact angles and unknown surface cavity dimensions. But, an attempt was made to theoretically calculate the bubble departure diameter from a force balance on the growing bubble. A more extensive description of the forces acting on a growing bubble is described in Furberg (2006), but as a summary, the force balance on the growing bubble may be estimated from following equations:

The upwardly directed buoyancy force, F_B, can be written according to the Archimedes principle:

$$F_B = (\rho_{liq} - \rho_{vap}) g V_{bubble} \approx \rho_{liq} g V_{bubble} \qquad (30)$$

The downwardly directed surface tension force, F_σ, can be written as:

$$F_\sigma = L_\alpha \sigma \sin\alpha \qquad (31)$$

where α is the bubble contact angle along a contact line with the length, L_α. The bubble contact angle is defined as the angle of the liquid wedge formed between the substrate and the bubble. L_α was assumed to be the top pore circumference of the structure (100 μm top pore diameter).

Surface tension gradients, resulting from temperature differences along the bubble surface, result in a downward directed net force, $F_{\Delta\sigma}$, on the bubble since the surface tension is lower at higher temperatures. The force may be estimated by:

$$F_{\Delta\sigma} \approx R\left(\sigma(T_{high}) - \sigma(T_{low})\right) = R\Delta\sigma \qquad (32)$$

where the measured surface temperature was used for T_{high} and the liquid saturation temperature was used for T_{low}.. Hence, the difference in temperature, causing the surface tension gradient, is the measured ΔT.

The downwardly directed liquid inertia force, $F_{liq\_inertia}$ developed during the growth of a bubble is the result of putting the surrounding fluid into motion. The shape and the growth rate, u, of the bubble will decide the magnitude of the inertia force, according to:

$$F_{liq\_inertia} = \frac{d}{dt}\left(m_{liq} u\right) \qquad (33)$$

where m_{liq} is the mass of the liquid that is being displaced by the growing bubble. A number of assumptions must be made to get a qualitative understanding for the liquid inertia force. The bubble shape is assumed to be spherical (quite close to the cylindrically shaped vapor front into the porous structure) and the time-dependency of the bubble radius, R, is assumed to be (uniform since the bubble is maintaining its spherical form) according to:

$$R = Ct^n \qquad (34)$$

where t is the time since bubble formation and n is the growth exponent, which varies throughout the growth period of the bubble, but is often found to be around ½, Hetsroni (2006). C is the growth constant [$m/s^{1/2}$] which depends on the particular physical conditions. Assuming $n = 1/2$ the liquid inertia force will be time independent and take the form:

$$F_{liq\_inertia} = A\pi\rho_{liq} C^4 \qquad (35)$$

where the constant A, theoretically, can be shown to be approximately 1/3 according to Slooten (1984). Since the bubble departing diameter was measured and the bubble frequency was calculated, the growth constant, C, can be calculated. Since the bubble growth rate increases with heat flux, so does the growth constant, C, which was found to be a function of heat flux approximated according to:

$$C = 1.53 \cdot 10^{-5} \cdot q''^{0.374} \qquad (36)$$

Similarly, the upwardly directed vapor inertia force, $F_{vap\_inertia}$, may be calculated as:

$$F_{vap\_inertia} = \frac{d}{dt}\left(m_{vap}u\right) \qquad (37)$$

Assuming that the growth rate of the bubble is governed by equation (34) and with a growth exponent, n = 1/2, the vapor inertia force may be calculated according to:

$$F_{vap\_inertia} = \frac{2}{3}\pi\rho_{vap}C^4 \qquad (38)$$

To roughly estimate the downward acting viscous drag force, F_D, on a growing bubble, it can be assumed that the bubble behave as a spherical bubble rising through the liquid with a velocity, u, equal to its change of radius with time according to equation (34). With a growth exponent, n = 1/2, and calculating the drag coefficient from a free rising bubble, the expression for the drag force becomes:

$$F_D = 6\pi\rho_{liq}\nu C^2 \qquad (39)$$

where ν is the liquid kinematic viscosity.

Thus, with equations (30) to (32), it is possible to calculate the bubble departure diameter. The bubble contact angle is unknown, but using a least square approach, it was calculated to 0.4°. The calculation of the contact angle is very sensitive to the contact line length, which is very hard to estimate. But, the micro-porous structure appears to have a very low contact angle (close to zero). The change in contact angle is probably the main reason for the smaller bubble departure diameter from the micro-porous surface compared to that of a plain surface, as could also be seen in the in appendix III. The calculated and measured bubble departure diameter is shown in Figure 46. According to this

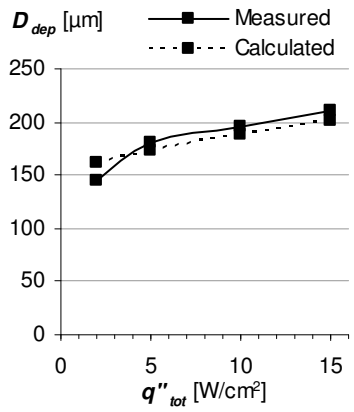

Figure 46. Calculated and measured bubble departure diameter vs. total heat flux.

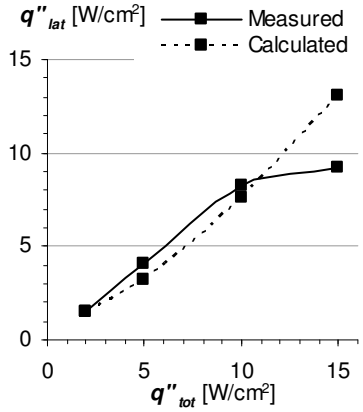

Figure 47. Calculated and measured latent heat transfer vs. total heat flux.

analysis, the bubble lift force is dominated by the bubble buoyancy and the downward acting forces are dominated by surface tension forces.

If a constant liquid film thickness of 3.7 μm is assumed (about average for all heat flux as seen in Figure 45) and the departure diameter is calculated for each heat flux as shown above, then the latent heat transfer may be calculated according to equation (28). The result is shown in Figure 47. As seen, the model predicts the latent heat flux quite well up to 10 W/cm^2. At 15 W/cm^2 the model over predicts the latent heat flux, the reason for which is unknown. But, it could be due to changes in the hydrodynamics at higher heat flux, for instance; a decrease in bubble contact angle. The dynamic contact angle is known to be dependent on the velocity, as seen in Mukherjee and Kandlikar (2006) and is decreasing with increasing vapor velocities, which would be the case at higher heat flux.

Single-phase Heat Transfer

Single-phase, or sensible, heat transfer is here defined as the heat that is transferred into liquid inside and outside the structure and that is not further transferred into the bubble within the structure or immediately after bubble departure. Some of this heat is either transferred into the bubbles as they rise through the superheated liquid, or as they travel toward the free liquid surface, or evaporated at the free liquid surface during the pool boiling experiments. The sensible heat transfer may be assumed to take place inside and on the top of the porous structure as liquid agitation is induced by the growing and departing bubbles as well as the net liquid flow into the structure.

Assuming that single-phase heat transfer is taking place on the entire surface of the dendritic branch structure, and that the dendritic branch structures are fins that acts as an extended surface, the sensible heat flux related to the top projected surface area, may be calculated as:

$$q''_{sens} = \frac{Q'_{sens}}{A_{top\_proj}} = h_{sens\_structure} \cdot f_{area} \cdot \eta_{fin} \cdot \Delta T \qquad (40)$$

where, $h_{sens\_structure}$, is the sensible heat transfer coefficient and the fin efficiency, η_{fin}, as defined and calculated in equations (21) through (25). The liquid convection is assumed to be caused by the agitation of vapor bubbles inside of the porous layer and the oscillating vapor front. A Nusselt number may be defined as:

$$Nu_{dh} = \frac{h_{sens\_structure} \cdot D_{fin}}{\lambda_{liq}} \qquad (41)$$

where D_{fin} is the diameter of the dendritic branches, which was estimated to about 1 μm, as described earlier in conjunction with equation(24). Assuming that fully developed flow does not form considering the irregular shape of the dendritic structure and the reversing of the flow direction with the moving of the vapor front, the Nusselt number, Nu_d, for external flow could be calculated from the general form of:

$$Nu_d = C \cdot Re_D^{\,m}\, Pr^n \qquad (42)$$

Where C, m and n are constants determined by the geometry and flow conditions and the Reynold number, *Re. Pr* is the Prandtl number of the fluid. External flow over a body at low Reynolds numbers with constants: $C = 1/3$, $m = 1/2$ and $n = 1/3$, Incropera and DeWitt (2002), was used as a first estimate. The Reynolds number was calculated according to:

$$Re_D = \frac{u \cdot D_{fin}}{\nu} \qquad (43)$$

where u is the liquid flow velocity inside the porous structure and ν is the kinematic viscosity and. Since the growth and departure of each bubble move the liquid inside the structure, the liquid velocity could be estimated with the distance the vapor advances with each oscillation (for each bubble), ΔR_{vap} , and the bubble oscillation frequency, f_{Hz} , (bubbles/pore/s). The total length the vapor front moves is twice that of ΔR_{vap} , hence:

$$u = 2\Delta R_{vap} \cdot \frac{f_{Hz}}{P} \qquad (44)$$

ΔR_{vap} was calculated with equations (17) and (19). The oscillation frequency per pore, f_{Hz}/P, was calculated with equation (29).

It is thus possible to calculate the sensible heat flux, q''_{sens}, using equations (40) through (29) and compare with the measured sensible heat flux results from the visualization study presented in appendix III. The calculated and measured sensible heat flux is presented in Figure 48 as a function of the total heat flux, q''_{tot} . Despite its simplicity, the model appears to capture both the trend and magnitude of the single-phase heat flux quite well. These results lend further support to the observation noted in appendix III, that: the single-phase heat transfer mechanism is significantly enhanced by the micro-porous structure due to the strong convection caused by the agitation of the vapor bubbles inside,

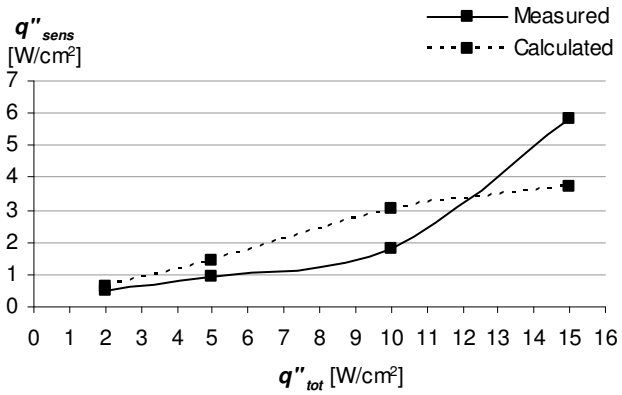

Figure 48. The calculated and indirectly measured sensible heat flux as a function of total heat flux.

and immediately outside, the porous layer.

As a summary, the latent and sensible heat transfer coefficients were calculated and added according to the superposition model for the 250 μm thick surface layer tested in appendix III. As described above, the liquid film thickness was assumed to be 3.8 μm on average and the contact angle 0.4°. The result is shown in Figure 48 which shows a quite good agreement between model and calculation. Figure 48 also includes the calculated heat transfer coefficient for a micro-porous structure with a 120 μm layer thickness. The same film thickness of 3.8 μm was assumed as well as the same contact angle. The surface area enlargement, f_{area}, and the fin length calculation were adjusted proportionally to the surface thickness, which agreed well with SEM pictures of the 120 μm thick dendritic and micro-porous surface layer. The nucleation density was assumed to be the same as for the 250 μm thick layer. The calculated heat transfer coefficient for the 120 μm thick surface layer was about 40% lower than for the 250 μm thick layer. Earlier experiments, as seen in appendix I, show a slightly smaller difference of about 25%, but the trend and behavior of the calculation model appears to be right.

Assumptions and Simplifications

A summary of the main assumptions and simplifications in the model:

- the main two-phase heat transfer mechanism inside the porous structure is: micro-layer evaporation formed by an oscillating vapor-liquid meniscus front with low resistance vapor transport through escape channels.
- the vapor escape channel is left filled with vapor after a departing bubble.
- the vapor is generated through thin film evaporation inside the porous structure
- the thickness of the thin liquid film is homogenous on the heat transfer

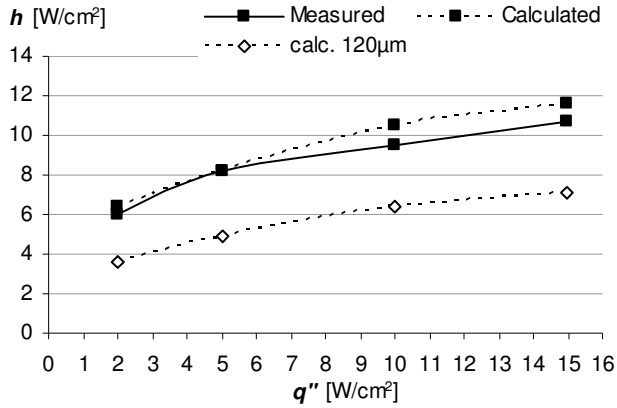

Figure 49. The calculated (both for the 250μm and 120μm thick surface layer) and measured heat transfer coefficient (250 μm thick layer) as a function of total heat flux.

surface on the dendritic branches.

- the liquid film thickness is the average thickness throughout half the time of the entire bubble cycle.
- the single-phase heat transfer mechanism is laminar liquid motion induced by the oscillating vapor front.
- liquid viscous effects of the advancing vapor front, liquid and vapor momentum forces, the permeability of the porous structure, and surface tension effects have not been taken into account.
- the geometrically complex shape of the dendritically ordered extended surface features is approximated with pin fins for the fin efficiency calculations.

The accuracy of this model is expected to be low and the results are highly sensitive to some input, especially that of the fin efficiency calculation, the surface area measurement and the bubble departure diameter.

Conclusions

A semi-empirical model was presented for the two- and single-phase heat transfer mechanisms in the dendritic structure. The accuracy of this model is expected to be low and the results are highly sensitive to some input, especially that of the fin efficiency calculation, the surface area measurement and the bubble departure diameter. It must be emphasized that the model is meant to serve as a basis for discussion around the boiling mechanisms involved within the structure.

Despite the rather large number of estimates and assumptions, the calculations lend some support to the hypotheses regarding the boiling heat transfer mechanisms in the dendritic structure. The model does not prove the hypothesis, but it shows that the suggested heat transfer mechanisms are a possibility.

Future work might take the model a step further and conduct more detailed simulations, possibly using CFD in conjunction with a more elaborate description and property measurement of the porous structure, such as permeability and thermal conductivity.

Nomenclature

A	area [m^2]
ΔA	area change [m^2]
α	bubble contact angle [rad]
B	bubble
D_d	the bubble departure diameter [m]

d_h hydraulic diameter of passageways between dendritic branches in the micro-porous structure [m]

δ_{film} liquid film thickness [m]

$\Delta\delta_{film}$ change in liquid film thickness with every bubble period [m]

f_{area}, area enlargement factor

f_{Hz} bubble oscillation frequency [s^{-1}]

H height of porous layer [m]

h heat transfer coefficient [W/ (m^2 K)]

λ thermal conductivity [W/(m K)]

L length [m]

L_α length of bubble contact line [m]

ϕ porosity of the porous structure [-]

ν kinematic viscosity [m^2/s]

q'' heat flux [W/m^2]

Q' heat flow rate [W]

η ratio between active pores and total number of pores

η_{fin} fin efficiency of porous structure branches

Nu Nusselt number

P Top pore in micro-porous structure

Pr Prandtl number

P_ρ pore density [P / A_{top_proj}]

Re Reynold number

R bubble radius [m]

ΔR_{vap} distance that vapor front advances [m]

ρ density [kg/m^3]

ΔT temperature difference [K]

u liquid flow velocity inside the porous structure [m/s]

ν kinematic viscosity [m^2/s]

V_{bubble} bubble volume [m^3]

V_{liq_evap} evaporated liquid volume corresponding to V_{bubble} [m^3]

Subscripts

film	liquid film
fin	fin
ht	heat transfer
lat	latent
liq	liquid
max	maximum
nμp	dendritic and micro-porous surface
structure	micro-porous structure
sens	sensible
vap	vapor
top_proj_wall	top projected wall structure
top_proj	top projected

7 Application of the Porous Structure in a Plate Heat Exchanger

As seen in appendix IV, the nano- and micro-porous copper structure was used to enhance the boiling heat transfer mechanism in the refrigerant channel of a gasket sealed plate heat exchanger. Figure 50 and shows the stainless steel heat exchanger plates, featuring a herringbone like macro-corrugation pattern with sinusoidal shape, which were assembled between two end frame plates and compressed by tightening bolts. Two distance frames in the refrigerant channel, 5 and 10 mm thick, were also employed to study the influence of the refrigerant mass flux and channel geometry on two-phase flow heat transfer as indicated in

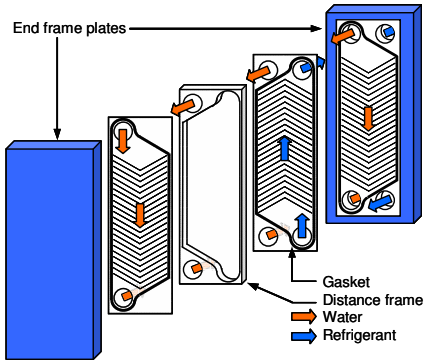

Figure 50. Plate heat exchanger with gasket seals and distance frame.

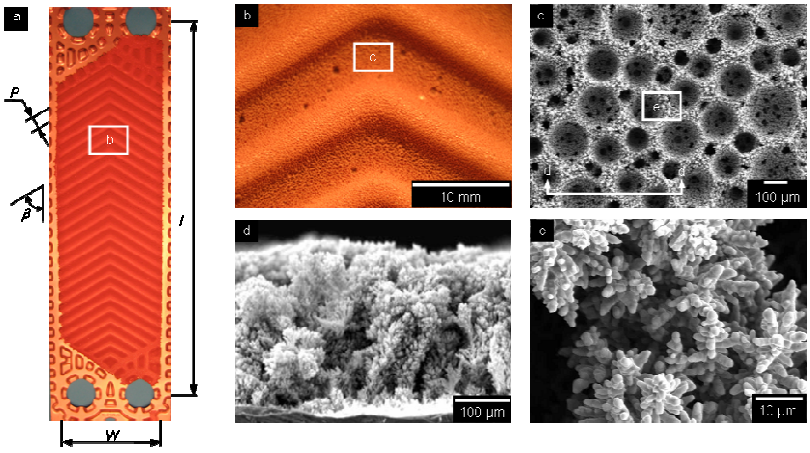

Figure 51. a. Heat exchanger plate with enhanced surface structure fabricated on the refrigerant side. b. Close-up view of enhanced heat exchanger plate. c. and e. SEM picture of the enhancement structure. d. SEM side-view.

Figure 50. Hence, in total; six heat exchanger configurations were tested.

The stainless steel heat exchanger plates were first pre-coated with a thin copper layer before the porous structure was manufactured on the surface. As seen in Figure 51, the porous layer took on a red shade and covered the complete sinusoidal shape. The diameter of the macro-pores gradually increased with distance from the substrate and had an average top layer diameter of 105μm as seen in Figure 51c. The thickness of the surface layer measured 250 μm and the top pore density of about 30/mm² (75/mm² was erroneously stated in the published article, appendix IV). The porous wall consisted of dendritically shaped structures forming a large surface area and numerous cavities between its branches. The overall porosity of the surface structure was about 95%, based on the measured thickness and mass of the surface layer and the density of solid copper. The coated plates underwent an annealing treatment before installed into the heat exchanger.

The tests were conducted with R134a and at heat fluxes ranging between 5 and 17 kW/m². The flow direction of the water and the refrigerant was counter-current. The water side flow rate through the test object corresponded to a temperature drop from 12.0-7.0 °C. The incoming vapor quality was controlled to 5-15%. Results from preliminary tests showed that difference in inlet quality between 5 and 15% had a negligible effect on the heat transfer coefficient on the refrigerant side. The outgoing vapor quality was controlled with the refrigerant pump to near 100% by decreasing the refrigerant flow until the measured superheat was 0.0°C. In order to evaluate the heat transfer performance on the refrigerant side, the heat transfer coefficient on the water side of the plates was first evaluated using a modified Wilson plot method during which the plates in the heat exchanger were configured to form two channels.

As seen in Figure 52, the enhanced surface structure in the refrigerant channel improved the overall performance of the heat exchanger, the U-value, with 68-108% compared to the STD configuration. The U-value for the nμP+10 configuration was only 10-20% below the maximum limit; where the thermal

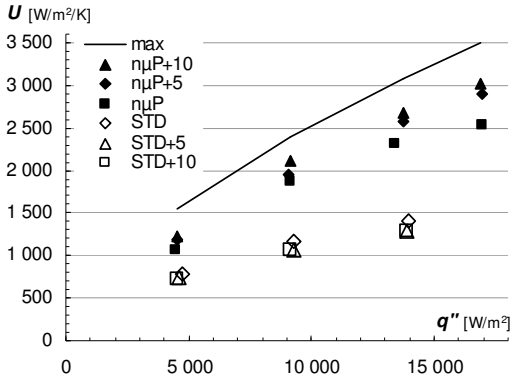

Figure 52. Overall U-value as a function of heat flux for standard and enhanced heat exchangers. nμp (micro-porous surface), STD (standard surface), +5 and +10 indicates the thickness use of the distance collar used.

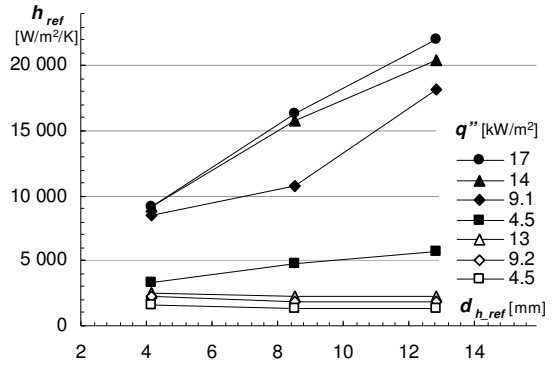

Figure 53. Heat transfer coefficient on refrigerant side, h_{ref}, as a function of the hydraulic diameter of the refrigerant channel, d_{h_ref}.
(Filled symbols – coated plates, white symbols – standard plates)

resistance on the refrigerant side is zero. In the standard heat exchanger, the thermal resistances on the water and refrigerant sides were comparable, but with the enhancement structure, the thermal resistance was about 4 to 7 times larger on the water side compared to the refrigerant side. Hence, it would be desirable to increase the heat transfer coefficient on the water side in a real application, to fully utilize this improvement in boiling heat transfer.

As seen in Figure 53, the enhanced plate heat exchanger exhibited an enhancement of the heat transfer coefficient in the refrigerant channel, h_{ref}, with up to 10 times. The introduction of a distance frame had a slightly negative effect (less 12% - 17%) on the refrigerant side heat transfer coefficient in the standard heat exchanger. The opposite trend was seen for the enhanced refrigerant channel, where the introduction of a 10 mm distance frame improved the refrigerant side heat transfer coefficient with 70% - 140%, approaching that of earlier pool boiling experiments. To test the influence of oil in the refrigerant, 2% (by weight) of compressor oil was added (Bitzer, BSE 170). The performance was the same as without oil.

As expounded upon in appendix IV, a superposition model was used to evaluate the results. The refrigerant side heat transfer coefficient, h_{ref}, was thus calculated as the sum of a convective boiling term, h_{cb}, and nucleate boiling term, h_{nb}, according to:

$$h_{ref} = h_{cb} + h_{nb} \quad (45)$$

For the standard plate heat exchanger configuration, Cooper's nucleate boiling correlation was used for the nucleate boiling heat transfer coefficient and the Dittus–Boelter correlation for the convective boiling term. The model correlates well with the experimental results. On average, the absolute deviation between the calculated and the measured refrigerant side heat transfer coefficient, h_{ref}, was only 2.2 %, with a maximum difference of 4.6%. The negative effect that distance frames on the convective boiling mechanism in the standard heat exchanger was also well captured by the model.

With the enhanced boiling structure applied to the plates, the Cooper's correlation for the nucleate boiling heat transfer coefficient did not satisfactory capture the nucleate boiling characteristics of the enhanced boiling surface and was therefore replaced with a logarithmic function of the heat flux. With the enhance structure, the variation in hydraulic diameter in the refrigerant channel was found to have caused a significant change in the boiling mechanism, as seen in Figure 53. This behavior was captured by a boiling suppression multiplier which was dependent on the dimensionless confinement number, defined as:

$$Co = \frac{\sqrt{\sigma / \left(g\left(\rho_{liq} - \rho_{vap}\right)\right)}}{d_{h\_ref}} \quad (46)$$

where σ is the liquid surface tension, ρ_{liq} and ρ_{vap} is the fluid density of the liquid and vapor respectively and d_{h_ref} is the hydraulic diameter of the refrigerant channel. The hydraulic diameter of the refrigerant flow channels was calculated according to:

$$d_{h\_ref} = \frac{2B + t_{frame}}{\phi} \quad (47)$$

where B is the plate corrugation depth, t_{frame} the thickness of the distance frame and ϕ the surface enlargement factor. Kew and Cornwell (1997) introduced the dimensionless confinement number, Co, and suggested that with Co>0.5, a bubble is confined in a small channel, which could affect the dominant heat transfer mechanism. Even though the average confinement number is a bit less than 0.5 for the three different configurations (0.22 without distance frame), local confinement effects are probably present in the channel due to the macro corrugation pattern, particularly when no distance frame was used. Thus, the channel walls appear to confine the rising vapor bubbles at small hydraulic diameters. These confined bubbles may have disrupted the otherwise highly active nucleation sites in the porous layer, causing temporary and local dry out of the dendritic structure. A similar behavior of the nano- and micro-porous structure was observed in flow boiling experiments in a thermosyphon loop, as seen in publication V.

Conclusions

The study is an example of a very successful application of the enhancement surface to a commercial heat exchanger. Just as in previous pool boiling tests, high boiling heat transfer enhancement ratios were recorded in this flow boiling application. No other studies have been found where the heat transfer coefficient on the refrigerant channel in plate heat exchangers was enhanced to the same level as in this study. The work confirmed that the structure may be applied to non- flat surface and refrigerant with oil, which is important for its industrial applicability. The importance of effective vapor removal from the structure through the vapor escape paths, which had been shown in the publication in appendix I, was yet again confirmed in the positive influence of a refrigerant channel with large hydraulic diameter.

8 Application of the Porous Structure to a Thermosyphon Evaporator

As seen in appendices V and VI, the dendritic and micro-porous structure was applied to the evaporator surface in a two-phase thermosyphon. In relation to this thesis work, the purposes of these tests were: to measure the performance of the micro-porous structure in a mini-channel application, to visualize the boiling on the micro-porous structure in narrow channels, to see if and how the boiling characteristics of the micro-porous evaporator affected to performance and stability of en entire thermosyphon.

Figure 54 shows the thermosyphon loop and some of its important dimensions. In order to investigate the influence of liquid level on the performance and instability of the thermosyphon system, the liquid levels of 33, 53 and 73 cm were tested as indicated in Figure 54. To further understand the instability, the tests were run with one steel tube riser with 8 mm inner diameter and three different glass tube risers with 10, 7.7 and 4 mm inner diameter. All test were conducted at Tests were conducted with R134a as the working fluid at a pressure of 6.5 bar, and a saturation temperature of approximately 24.2 °C.

The publication in appendix V reports the results from the first series of tests. In these experiments, the liquid riser level was at 53 cm and had an inner

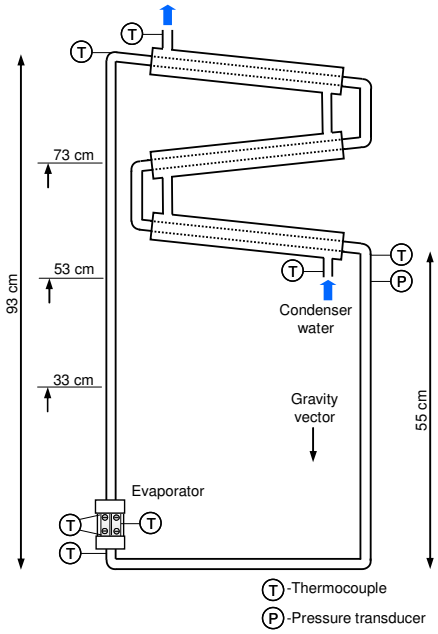

Figure 54. A schematic drawing of the advanced thermosyphon loop with water cooled condenser.

diameter of 8 mm. Six different evaporators were tested; five smooth evaporator surfaces with channels of various hydraulic diameters and one evaporator with the dendritic and micro-porous surface structure applied to the channel. Geometrical details of the tested evaporator surfaces are presented in Table 1. To facilitate high speed video visualization of the two-phase flow in the evaporator channel, a transparent polycarbonate window was attached to the front of the evaporators, as seen in Figure 55.

As seen in Figure 56, the tests showed that increasing channel diameters generally exhibited higher heat transfer coefficients for the smooth channels. The three largest evaporator channels exhibited comparable performance, with a maximum heat transfer coefficient of about 2.2 W/(cm^{2}K) at a heat flux of 30-35 W/cm^2 and a critical heat flux of around 50 W/cm^2.

Three general flow regimes were observed for the smooth surfaces;

- bubbly flow with nucleate boiling heat transfer mechanism where heat transfer increased with increasing heat flux
- confined bubbly/churn flow with backflow and low heat transfer coefficient;
- churn flow at high heat fluxes with convective evaporation.

Isolated bubbles were found to characterize the flow regime at peak performance for the large diameter channels, while confined bubbles and chaotic churn flow typified the evaporators with small diameters. These visual observations agree well with Kew and Cornwell's (1997) confined boiling

Table 1. Dimensions, hydraulic diameter, D_h, and heat transfer surface area of the tested evaporators. Smooth surfaces are denoted with s, and the micro-porous surface is denoted nμp.

Evaporator	*L* [mm]	*H* [mm]	*w* [mm]	D_h [mm]	*A* [cm^2]
***s*-0.7**	30.0	0.7	5.0	1.2	1.92
***s*-0.9**	30.0	0.9	5.0	1.6	2.07
***s*-1.3**	30.0	1.3	5.1	2.1	2.30
***s*-1.6**	30.0	1.6	5.1	2.4	2.49
***s*-1.8**	30.0	1.8	5.3	2.7	2.68
***nμp*-1.7**	30.0	1.7	5.1	2.5	2.50

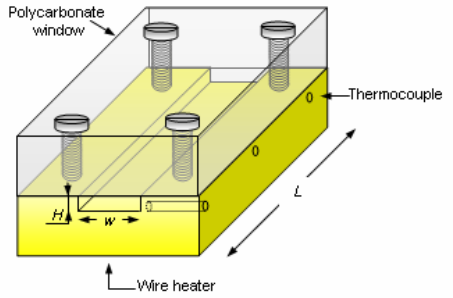

Figure 55. A detailed view of the evaporator with the polycarbonate window.

criteria based on the confinement number, Co, as seen in equation (46). The predicted threshold diameter was calculated to 1.7 mm under the conditions of these tests. The confined bubble flow regime was characterized by large fluctuations in the flow pattern with bubbles forming at the inlet of the channel seemingly blocking the liquid flow through the evaporator and thereby causing poor heat transfer performance. The highest heat transfer coefficients were recorded when the nucleate boiling mechanism was dominant, while confined boiling and churn like flow resulted in lower heat transfer coefficients.

The evaporator channel with the micro-porous surface structure had a hydraulic diameter of about 2.5 mm. The micro-sized pores had an average top layer pore diameter of about 110 μm with an approximate pore density of 30 pores/mm^2. The thickness of the surface layer measured about 250 μm. The nucleate boiling mechanism was enhanced by the micro-porous structure, as seen in Figure 56. The improvement of the heat transfer coefficient of up to 4 times is comparable to the enhanced plate heat exchanger with the smallest hydraulic diameter, of 4.2 mm, tested in publication IV. In the heat flux range of 0 - 25 W/cm^2, the high speed videos of the enhanced evaporator reveal an isolated bubble flow regime, similar to that of the larger smooth channels.

Since it has been shown that the structure effectively enhances the boiling mechanism in pool boiling, the sharp increase of the heat transfer coefficient was expected. But, at higher heat fluxes, the heat transfer coefficient rapidly decreased, indicating a change in the effective boiling mechanism. At about 25W/cm^2 the heat transfer coefficient rapidly decreases, indicating a change in

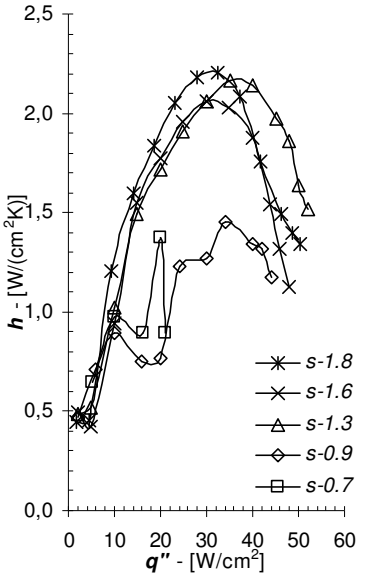

Figure 56. Heat transfer coefficient vs. heat flux for smooth evaporator channels of various depths.

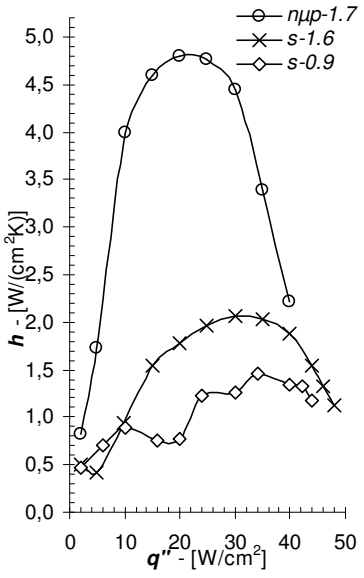

Figure 57. Heat transfer coefficient vs. heat flux for the enhanced evaporator. Two smooth evaporators are also shown for comparison.

the effective boiling mechanism. The pores of the micro-porous structure can be clearly seen at the centre of the channel. This absence of bubble nucleation sites in the centre of the channel indicates that the nucleate boiling mechanism is negatively affected at these higher heat fluxes. But, at heat flux above 25 W/cm^2, active pores generating bubbles were still visible all along the sides of the vertical channel. From studying the high speed videos, it appears that the vapor fraction in the centre of the channel is very high, which indicates that there is a partial dry-out of the evaporator surface already at 25 W/cm^2. The highly effective evaporation that takes place in the enhanced structure generates a large vapor flow. Hence, the liquid flow in this particular thermosyphon configuration was too low to take full advantage of the enhanced structure. The critical heat flux for the enhanced surface was found to be about 40 W/cm^2, which was about 20% lower than that of the smooth surface. (This suggested explanation of the rapidly declining heat transfer coefficient with the micro-porous surface at heat flux above 25 W/cm^2, differs slightly from the one given in the publication in appendix V)

As seen in the test series in appendix VI, glass risers with varying inner diameters (4, 8 and 10 mm) were installed in the thermosyphon to further understand the observed flow instabilities. The influence of the liquid level and the inside diameter of the riser on the instability of the system were investigated. Two different types of density wave oscillations causing instabilities were observed. Both occurred due to an inefficient heat transfer in boiling and evaporation, but for different reasons.

Density wave oscillations at low heat fluxes; type 1 instabilities, were mainly caused by backflow of (subcooled) liquid from the riser and also condensed vapor in the evaporator with flow stagnation in evaporator in the first step and totally collapse of vapor in the second step which gave single-phase flow in evaporator with much lower heat transfer. In the third step, the bubbles initiated, grew and departed from the surface and thereby cooled down the evaporator wall. This instability resulted in fluctuations in evaporator wall temperature. As seen in Figure 58, the amplitude of the temperature fluctuations were about twice as large for the evaporator with the smooth surface compared to the micro-porous evaporator.

Type II instability occurred at high heat fluxes at relatively high friction two-phase flow pressure drop at slug/churn flow regime with convective heat transfer mechanism. This instability with high heat fluxes was related to disturbed nucleate boiling and occurrence of hot dry spots and also convective mechanism of the heat transfer. As the vapor quality increased and the boiling suppressed, dry patches formed locally and the wall temperature increased. Temperature measurements in three different locations in the evaporator channel showed that the heat transfer at the inlet was more efficient with lower wall temperature, as compared to the middle and outlet of the evaporator where dry patches formed. With these type II instabilities, the temperature of the evaporator fluctuated, due to dry-out and rewetting of evaporator wall surface. But again, the amplitude of the temperature fluctuations were more than twice as large for the evaporator with the smooth surface compared to the micro-porous evaporator.

The high speed videos showed that the number and frequency of the produced bubbles were significantly higher for the enhanced surface. This enhanced turbulence and continuous boiling with high frequency generated enough bubbles to cause sufficient density difference between riser and down-comer to ensure the required mass flow for the smooth running of the thermosyphon system. Hence, the enhanced structure surface decreased the oscillations at the entire range of heat fluxes

Higher liquid level in the riser improved the performance of the thermosyphon and suppressed fluctuations. It was found that, the larger the cross-section of the riser the more oscillation occurred in the evaporator, due to lower flowing force to lift up the liquid in the riser to the condenser. Generally; at lower liquid level and larger diameter of the riser at low heat fluxes, the liquid in the riser did not flow over into the condenser inlet, rather the bubbles and slugs collapsed in the riser and built up a fluctuating liquid column in the riser.

Conclusions

The application of the dendritic and micro-porous surface layer to the evaporator in a thermosyphon resulted in an improvement in heat transfer coefficient. The improvement in heat transfer coefficient compared to a smooth reference surface of 4 times was similar to the enhanced plate heat exchanger with the smallest hydraulic diameter. The application of the micro-porous structure to the evaporator surface also decreased the amplitude of oscillations in the thermosyphon and thereby improved the operation and the reliability of the entire system. High speed filming yielded, for the first time, valuable information regarding the flow boiling characteristics of the micro-porous surface. It was clear from these videos that vapor generation inside the porous structure caused the high heat transfer performance, which was seen in the high

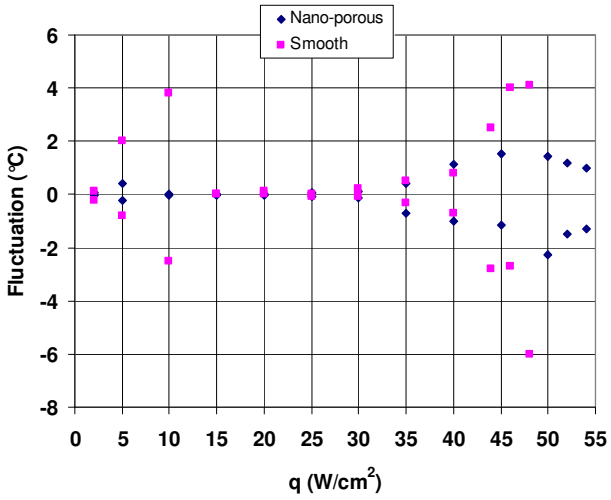

Figure 58. Fluctuation of evaporator temperature at different heat fluxes with 7.7 mm diameter riser of for micro-porous and smooth surfaces.

bubble density and frequency.

9 Concluding Remarks and Recommendations

Unique Contribution

Some of the unique features of this thesis work, other being an example of a fruitful collaboration between the disciplines of thermodynamics and material science have been its; width, depth, innovativeness and industrial applicability.

Widths: The work contains elements of nanotechnology, surface characterization, chemical fabrication technologies, both pool and film boiling experiments, high speed video of miniature objects, thermosyphon behavior, theoretical modeling and analysis of different boiling modes, as well as several fundamentally different experimental constructions. The variety of applications tested and the many number of different structures produced on various metallic substrates are quite exceptional, such as; on 1 mm narrow ridges, 320 cm^2 large plates, 5 mm wide and 1.7 mm deep channels, round objects, wavy objects and rectangular objects.

Depth: The detailed with which the surface structure has been pictures and documented and many different boiling tests performed has resulted in a picture that is multifaceted. The rarity of boiling tests of a micro-porous surface structure documented with a high speed camera provides detailed data than in conjunction with a rigorous analysis has provided a level of understanding of the underlying boiling mechanisms than what is normally the case in these kinds of studies.

Innovativeness: To first and foremost generate new and good ideas and then realizing them requires an ability to innovate. Good innovations often come from merging insights from different fields. This thesis project has been characterized by innovation from beginning to end, with the development of the methods for the creation of the surface structure and its use in boiling applications as one example. Another example is the application of this surface structure to various substrates, a story that contains many twists and turns. Some of these innovations are captured in patent applications; others are stored away as tacit know-how.

Industrial applicability: With the advent of more precise and cost effective fabrication methods for enhanced surfaces for boiling, the level of activity within the field is high. The potential benefits of miniaturization, improved energy efficiency of systems, enhanced safety and reliability and more cost effective solutions are driving the development. The future will tell if the surface structure presented in this thesis work eventually finds its way into useful applications, but the odds good. Patent applications have been filed in the countries representing the world's major economies. A company, Micro Delta T, was started-up in 2006 as a result of the hitherto promising results and investors, public funders and customers have shown a steady interest.

This thesis work has resulted in several reviewed journal and conference publications, a licentiate thesis and a number of master theses. The work has contributed to the advancement of new knowledge in the fields of surface manufacturing and enhanced boiling. The surface structure is unique and the use of it as a boiling surface is novel and the extraordinary good boiling performance of the surface structure has revealed the importance of certain characteristics of an effective boiling surface. A boiling model have been developed to analyze the boiling mechanisms in and around the surface structure and engineering correlations have been suggested for the use of the surface in plate heat exchangers. This knowledge can be used and built on by others. The ambition has been to employ the scientific method in the use of systematic and reproducible measurement and experiment and in the formulation and testing of hypotheses.

Rather than reiterating findings and conclusions, a few concluding remarks will be made that are based on the research work presented in this thesis work.

Surface Fabrication and Characterization

- The electrodeposition process under high current densities followed by various annealing treatments and low current deposition is simple and complicated at the same time. There's plenty of room for improving the surface fabrication technique. The unique vapor escape channels formed by the dynamic hydrogen bubble mask and its similarity with the bubble cycle during boiling are crucial to the usefulness of the surface. The possibilities of altering the dimensions of these channels are many and more work is recommended be done in understanding the full impact of different structural features, such as the boiling performance of structures with different height and pore size.

- The characterization of the surface was mainly done with SEM imaging and weighing of the deposited amount. One attempt at surface area measurements, BET, was done. To further improve the understanding of various characteristics of the surface structure under various boiling conditions, accurate permeability and thermal conductivity measurements should be performed and coupled with boiling test performance.

Pool Boiling and Modeling

- The micro-porous surface structure has been shown to perform exceptionally well in pool boiling experiments. The influence on the heat transfer coefficient of the annealing treatment, vapor escape channels and the height of the structure were tested. A more in-depth study was also performed using high speed filming in both FC-72 and R134a. The results from the visualization study were also used as a basis for a simple pool boiling model based on the hypothesis of thin-film evaporation being the main two-phase heat transfer mechanism. To further the understanding of the boiling mechanism more visualization studies should be performed where the influence of various surface characteristics is tested (height, pore diameter,

thermal conductivity, etc). This would also aid in the development of different surfaces for different fluids. Testing the different surface under CHF conditions would also yield valuable information regarding the bubble hydrodynamics inside the structure.

- The presented boiling model is simple, but it appears to capture the basic physics of the heat transfer mechanism and is to be seen as a first basis from which more detailed analyses may be made. For future modeling efforts, it would be helpful to use CFD for some parts of the heat transfer and hydrodynamic phenomena within the structure, such as; the effect from viscous forces in the formation of liquid layers on a finger structure, liquid inertia effects at different heat flux, etc. CFD modeling coupled with a better described surface structure and more high speed boiling visualizations studies, would be of great value to the understanding and development of future boiling surfaces.

The Micro-Porous Surface Structure in Applications

- The surface structure was successfully applied to a standard gasket plate heat exchanger, resulting in a doubling of the overall UA-value. There are oil free compressors available on the market today, but the vast majority of evaporators still operate with oil dissolved in the refrigerant. The recommendations for next steps would be to perform tests in a compressor driven heat pump with oil. A test rig was built during the spring of 2011 and the first results indicate that there is no negative influence from oil in the refrigerant.

- Applying the surface structure to the evaporator in a thermosyphon loop and studying the boiling behavior with a high speed visualization system provided useful information regarding the flow boiling behavior of the porous structure, particularly at higher heat fluxes. For a surface structure with the height of around 200-300 μm, most on the enhancement is seen in the bubbly flow regime. The thermosyphon is quite suitable for visualization studies of flow boiling and could therefore be used in future research where surface with different dimensions and features are tested.

Finally, in enhanced boiling heat transfer, the researcher often has the opportunity to significantly improve the thermal performance of a heat transfer process. This improvement can rarely be obtained through following standard, ordinary design procedures, but rather through much creativity and innovation. Every heat exchanger is a potential candidate for enhanced heat transfer and herein lays much of the fun and the challenge with the research in this field.

10 References

Ahn, H.S., Sinha, N., Zhang, M., Banerjee, D., Fang, S., Baughman, R., 2006, *Pool Boiling Experiments on Multiwalled Carbon Nanotube (MWCNT) Forests*, Journal of Heat Transfer, 128, pp. 1335-1342.

Akapiev, G. N., Dmitriev, S. N., Erler, B., Shirkova, V. V., Schultz, A., Pietsch, H., 2003, *Ion Track Membranes Providing Heat Pipe Surfaces with Capillary Structures,* Nuclear Instruments and Methods in Physics Research Section B: Beam Interactions with Materials and Atoms, 208, pp. 133-136.

Chang, J. Y., You, S. M., 1996, *Heater Orientation Effects on Pool Boiling of Micro-Porous-Enhanced Surfaces in Saturated FC-72*, Journal of Heat Transfer, 118, pp. 937-943.

Chang, J. Y., You, S. M., 1997, *Boiling heat transfer phenomena from micro-porous and porous surfaces in saturated FC-72*, International Journal of Heat and Mass Transfer, 40, pp.4437-4447.

Chen, R., Lu, M., Srinivasan, V., Wang, Z., Cho, H.H., Majumdar, A., 2009, *Nanowires for Enhanced Boiling Heat Transfer*, Nanoletters, 9 (2), pp. 548-553.

Cooper, M. G., Lloyd, A. J. P., 1969, *The Microlayer in Nucleate Pool Boiling*, International Journal of Heat and Mass Transfer, 12, pp. 895-913.

Das, A.K., Das, P.K., Saha, P., 2009, "*Performance Of Different Structured Surfaces In Nucleate Pool Boiling*", Applied Thermal Engineering, 29, pp. 3643–3653.

Demiray, F., Kim, J., 2004, *Microscale Heat Transfer Measurements During Pool Boiling of FC-7: Effect of Subcooling*, International Journal of Heat and Mass Transfer, 47, pp. 3257-3268.

Dhir, V. K., 2001, *Numerical Simulations of Pool-Boiling Heat Transfer*, AIChE Journal, 47, pp. 813-834.

Dhir, V. K., 2006, Mechanistic Prediction of Nucleate Boiling Heat Transfer–Achievable or a Hopeless Task?, Journal of Heat Transfer, 128, Issue 1, 1 (12 pages), doi:10.1115/1.2136366.

El-Genk, M. S., Parker, J. L., 2005, *Enhanced boiling of HFE-7100 dielectric liquid on porous graphite*", Energy Conversion and Management, 46, pp. 2455-248.

Forrest, E., Williamson, E., Buongiorno, J., Hu, L., Rubner, M., Cohen, R., 2010, *Augmentation of nucleate boiling heat transfer and critical heat flux using nanoparticle thin-film coatings*, International Journal of Heat and Mass Transfer, 53, pp. 58–67.

Franco, A., Latrofa, E. M., Yahov, V. V., 2006, *Heat Transfer Enhancement in Pool Boiling of a Refrigerant Fluid with Wire Nets Strutures*, Experimental Thermal and Fluid Science, 30, pp. 263-275.

Furberg, R., 2006, *Enhanced Boiling Heat Transfer From a Novel Nanodendritic Micro-Porous Copper Structure*, ISSN 1102-0245, Licentiate thesis at Royal Institute of Technology, Stockholm, Sweden

Furberg, R., Li, S., Palm, B., Toprak, M., Muhammed M., 2006, *Dendritically Ordered Nano-Particles in a Micro-Porous Structure for Enhanced Boiling*, Proceedings of IHTC-13 conference, Sydney, AU.

Furberg, R., Khodabandeh, R., Palm, B., Li, S., Toprak, M., Muhammed, M., 2008, *Experimental Investigation of an Evaporator Enhanced With a Micro-Porous Structure in a Two-Phase Thermosyphon Loop*, Proceedings of 2008 ASME Summer Heat Transfer Conference, HT2008, August 10-14, Jacksonville, Florida USA.

Furberg, R., Palm, B., Li, S., Toprak, M., Muhammed M., 2009, *The Use of a Novel Nano- And Micro-Porous Structure For Enhanced Boiling In a Plate Heat Exchanger*, Journal of Heat Transfer (special edition on porous media heat transfer), Vol. 131 (10).

Furberg, R., March 2006, *Forces Acting on a Bubble*, Royal Institute of Technology, Sweden, Stockholm

Furberg, R., March 2010, *Enhanced Boiling – Literature Survey*, Royal Institute of Technology, Sweden, Stockholm.

Furberg, R., Palm, B., 2011, *Boiling Heat Transfer on a Dendritic and Microporous Surface in R134a and FC-72*, Applied Thermal Engineering, 31, pp. 3595-3603.

Ghiu, C. D., Joshi, Y. K., 2005, *Visualization Study of Pool Boiling from Thin Confined Enhanced Structures*, International Journal of Heat and Mass Transfer, 78, pp. 4287-4299.

Ghiu, C-D., Joshi, Y. K., 2005, *Boiling Performance of Single-Layered Enhanced Structures*, Journal of Heat Transfer, 127, pp. 675-683.

Han, Y., Shikazono, N., 2011, *The Effect of Bubble Acceleration on the Liquid Film Thickness in Micro Tubes*, International Journal of Heat and Fluid Flow, Vol. 31 pp. 630–639.

Hetsroni, G., Mosyak, A., Pogrebnyak, E., Sher, I., Segal, Z., 2006, *Bubble Growth in Saturated Pool Boiling in Water and Surfactant Solution*, International Journal of Multiphase Flow, 32, pp. 159-182.

Honda, H., Takamatsu, H., Wei, J. J., 2002, *Enhanced Boiling of FC-72 on Silicon Chips With Micro-Pin-Fins and Submicron-Scale Roughness*, Journal of Heat Transfer, 124, pp. 383-390.

Hsu, Y.Y., 1962, *On the size range of active nucleation cavities on a heating surface*, Journal of Heat Transfer, 84, pp. 207–213.

Hwang, G.-S., Kaviany, M., 2006, *Critical Heat Flux in Thin, Uniform particle Coatings*, International Journal of Heat and Mass Transfer, 49, pp. 844-849.

Höhmann, C., Stephan, P., 2002, *Microscale Temperature Measurement at an Evaporating Liquid Meniscus*, Experimental Thermal and Fluid Science, 26, pp. 157-162.

Incropera, F. P., DeWitt, D. P., 2002, Fundamentals of Heat and Mass Transfer, fifth edition, John Wiley and Sons.

Kew, P.A., Cornwell, K., 1997. *Correlations for the Prediction of Boiling Heat Transfer in Small-Diameter Channels*, Applied Thermal Engineering, 17, pp. 705-15.

Kim, Y., Lee, K., Han, D., 2008, "Pool boiling enhancement with surface treatments", Springer-Verlag, Heat Mass Transfer 45:55–60.

Kim, J. K., Rainey, K. N., You, S. M., Pak, J. Y., 2002, *Mechanism of Nucleate Boiling Heat Transfer Enhancement from Microporous Surfaces in Saturated FC-72*, Journal of Heat Transfer, 124, pp. 500-506.

Kim, J., 2009, *Review of nucleate pool boiling bubble heat transfer mechanisms*, International Journal of Multiphase Flow, pp. 1067 – 1076.

Kim, J., Kim, M., 2006, *On the Departure Behaviors of Bubble at Nucleate Pool Boiling*, International Journal of Multiphase Flow, 32, pp. 1269 – 1286.

Kim, N., Kim, D., 2010, "*Pool Boiling of R-123/Oil Mixtures on Enhanced Tubes Having Different Pore Sizes*", International Journal of Heat and Mass Transfer, 53, pp. 2311-2317.

Khodabandeh, R., Furberg, R., 2010, *Heat Transfer, Flow Regime and Instability of a Nano- and Micro-Porous Structure Evaporator in a Two-Phase Thermosyphon Loop*, International Journal of Thermal Sciences, pp. 1183 – 1192.

Launay, S., Fedorov, A. G., Joshi, Y., Cao, A., Ajayan, P. M., 2006, *Hybrid Micro-Nano Structured Thermal Interfaces for Pool Boiling Heat Transfer Enhancement*, Microelectronics Journal, 37, pp. 1158-1164 .

Li, C., Peterson, G.P., 2007, "*Parametric Study of Pool Boiling on Horizontal Highly Conductive Microporous Coated Surfaces*", Journal of Heat Transfer (ASME), 129, pp.1465-1475.

Li, S., Furberg, R., Toprak, M., Palm, B., Muhammed, M., 2008, *Nature-inspired Boiling Enhancement by Novel Nanostructured Macro-porous Surface*, Advanced Functional Material, Vol. 18, pp. 2215–2220.

Liao, J., Mei, R., Klausner, J. F., 2004, *The Influence of the Bulk Liquid Thermal Boundary Layer on Saturated Nucleate Boiling*, International Journal of Heat and Fluid Flow, 25, pp. 196-208.

Liter, S. G., Kaviany, M., 2001, Pool.Boiling CHF enhancement by modulated porous-layer coating: theory and experiment, International Journal of Heat and Mass Transfer, 44, pp. 4287-431

Ma, A., Wei, J., Yuan, M., Fang, J., 2009, *Enhanced flow boiling heat transfer of FC-72 on micro-pin-finned surfaces*, International Journal of Heat and Mass Transfer, 52, pp. 2925-2931.

Min, D.H., Hwang, G.S., Usta, Y., O.N., Koc, M., Kaviany, M., 2009, *2-D and 3-D modulated porous coatings for enhanced pool boiling*, International Journal of Heat and Mass Transfer, 52, pp. 2607–2613.

Mitrovic, J., Hartmann, F., 2004, *A New Microstructure for Pool Boiling*, Superlattices and Microstructures, 35, pp. 617-628.

Moghaddam, S., Kiger, K., 2008. *Physical Mechanisms Of Heat Transfer During Single Bubble Nucleate Boiling Of FC-72 Under Saturated Conditions – I. Experimental Investigation*,. Int. J. Heat Mass Transfer, 52, p. 1284–1294.

Mori, S., Okuyama, K., 2009, *Enhancement of the critical heat flux in saturated pool boiling using honeycomb porous media*, International Journal of Multiphase Flow, 35, pp. 946–951.

Myers, J. G., Yeramilli, V. K., Hussey, S. W., Yee, G. F.,. Kim, J., 2005, *Time and Space Resolved Wall Temperature and Heat Flux Measurements During Nucleate Boiling with Constant Heat Flux Boundary Conditions*, International Journal of Heat and Mass Transfer, 48, pp. 2429-2442.

Mikic, B.B., Rohsenhow, W.M., 1969. *A New Correlation Of Pool Boiling Data Ncluding The Effect Of Heating Surface Characteristics,* J. Heat Transfer 9, pp. 245–250.

Mitrovic, J., 1998, *The Flow and Heat Transfer in the Wedge-Shaped Liquid Film Formed during the Growth of a Vapor Bubble*, International Journal of Heat and Mass Transfer, 41, pp. 1771-1785.

Mitrovic, J., 2002, *On the Profile of the Liquid Wedge Underdneath a Growing Vapor Bubble and the Reversal of the Wall Heat Flux*, International Journal of Heat and Mass Transfer, 45, pp. 409-415.

Mitrovic, J., 2006, *How to Create an Efficient Surface for Nucleate Boiling*, International Journal of Thermal Sciences, 45, pp. 1-15.

Mukherjee, A., Kandlikar, S, 2007, *International Journal of Heat and Mass Transfer*, 50, pp. 127–138.

Nakayama, W., Daikoku, T., Kuwahara, H., Nakajima, T., 1980, *Dynamic Model of Enhanced Boiling Heat Transfer on Porous Surfaces, Part I: Experimental Investigation*, Journal of Heat Transfer, 102, pp. 445-450.

Nakayama, W., Daikoku, T., Kuwahara, H., Nakajima, T., 1980, *Dynamic Model of Enhanced Boiling Heat Transfer on Porous Surfaces, Part II: Experimental Investigation*, Journal of Heat Transfer, 102, pp. 451-456.

Nakayama, W., Daikoku, T., Nakajima, T., 1982, *Effects of Pore Diameters and System Pressure on Saturated Pool Nucleate Boiling Heat Transfer From Porous Surface*, Journal of Heat Transfer, 104, pp. 286-291.

O'Connor, J. P., You, S. M., 1995, *A Painting Technique to Enhance Pool Boiling Heat Transfer in Saturated FC-72*, Journal of Heat Transfer, 117, pp. 387-393.

O'Neill, P. S., Gottzmann, C. F., Terbot, J. W., 1971, *Novel Heat Exchanger Increases Cascade Cycle Efficiency for Natural Gas Liquefaction*, 68th National AlChE Meeting, Houston, Texas, pp. 420-437.

Parker, J.L., El-Genk, M.S., 2006, *Effect of Surface Orientation on Nucleate Boiling of FC-72 on Porous Graphite*, Journal of Heat Transfer, 128, pp. 1159-1175.

Pastuszko, R., 2008, "*Boiling Heat Transfer Enhancement in Subsurface Horizontal And Vertical Tunnels*", Experimental Thermal and Fluid Science, 32, pp. 1564–1577.

Phan, T. H., Caney, N., Marty, P., Colasson, S., Gavillet, J., 2009, *Surface wettability control by nanocoating: The effects on pool boiling heat transfer and nucleation mechanism*, International Journal of Heat and Mass Transfer,

Ramawamy, C., Joshi, Y., Nakayama, W., Johnson, W. B., 2002, *High-speed Visualization of Boiling from an Enhanced Structure*, International Journal of Heat and Mass Transfer, 45, pp. 4761-4771.

Ramawamy, C., Joshi, Y., Nakayama, W., Johnson, W. B., 2003, *Semi-analytical Model for Boiling from Enhanced Structures*, International Journal of Heat and Mass Transfer, 46, pp. 4257-4269.

Rainey, K. N., You, S. M., 2000, *Pool Boiling Heat Transfer From Plain and Microporous, Square Pin-Finned Surfaces in Saturated FC-72*, Journal of Heat Transfer, 122, pp. 509-516.

Rainey, K. N., You, S. M., 2001, *Effects of Heater Size and Orientation on Pool Boiling Heat Transfer from Microporous Coated Surfaces*, Journal of Heat Transfer, 122, pp. 509-516.

Schulz, A., Akapiev, G. N., Shirkova, V. V, Röstler, H., Dmitriev, S. N., 2005, *A New Method of Fabrication of Heat Transfer Surfaces with Micro-Structured Profile*, Nuclear Instruments and Methods in Physics Research Section B: Beam Interactions with Materials and Atoms, 236, pp. 254-258.

Schulz, A., Akapiev, A.K., Shirkova, V.V., Rösler, H., Dmitriev., S.N., 2008, *The overheat temperature for the boiling process on metallic surfaces with microstructured relief*, Radiation Measurements, 43, pp. S612–S616.

Scurlock, R. G., 1995, *Enhanced boiling heat transfer surfaces*, Cryogenics, 35, pp. 233-237.

Shin, H. C., Dong, J., and Liu, M., 2003, *Nanoporous Structures Prepared by an Electrochemical Deposition Process*, Advanced Materials, 15, pp. 1610-1614.

Shin, S., Abdel-Khalik, S. I., Jurik, D., 2005, *Direct Three-Dimensional Numerical Simulation of Nucleate Boiling Using the Level Contour Reconstruction Method*, International Journal of Multiphase Flow, 31, pp. 1231-1242.

Shin, S., Juric. D., 2002, *Modeling Three-Dimensional Multiphase Flow Using a Level Contour Reconstruction Method for Front Tracking without Connectivity*, Journal of Computational Physics, 180, pp. 427-470.

Slooten, P. C., 1984, *Departure of vapor- and gas-bubbles in a wide pressure range*, Doctoral Thesis, Technical University of Eindhoven, Netherlands.

Stephan, P., Hammer, J., 1994, *A New Model For Nucleate Boiling Heat Transfer*, Wäirme- und Stoffübertragung 30 119-125 © Springer-Verlag 1994

Stephan, P., Hammer, J., Dhir, V. K., and reponse by Mitrovic, J., 1999, *Letters to the Editor*, International Journal of Heat and Mass Transfer, 42, pp. 3719-24.

Theofanous, T.G., Tu, J.P., Dinh, A.T., Dinh, T.N., 2002, *The Boiling Crisis Phenomenon: Part II: Dryout dynamics and Burnout*, Experimental Thermal and Fluid Science, 26, pp. 793-810.

Theofanous, T.G., Tu, J.P., Dinh, A.T., Dinh, T.N., 2002, *The Boiling Crisis Phenomenon: Part I: Nucleation and Nucleate Boiling Heat Transfer*, Experimental Thermal and Fluid Science, 26, pp. 775-792.

Thome, J., 1990, *Enhanced Boiling Heat Transfer*, Hemisphere, New York.

Ujereh, S., Fisher, T., Mudawar, I., 2007, *Effects of carbon nanotube arrays on nucleate pool boiling*, International Journal of Heat and Mass Transfer, 50, pp. 4023–4038.

Vemuri, S., Kim, K., 2005, *Pool Boiling of Saturated FC-72 on Nano-Porous Surface*, International Communications in Heat and Mass Transfer, 32, pp. 27-31.

Wagner, E., Stephan, P., 2009. *High Resolution Measurements at Nucleate Boiling of Pure FC-84 and FC-32384 and Its Binary Mixtures*, Journal of Heat Transfer, 131, 121008.

Wayner, P. C., Kao, Y. K, LaCroix, L. V., 1976, *The Interline Heat-Transfer Coefficient of an Evaporating Wetting Film*, International Journal of Heat and Mass Transfer, 19, pp. 487-492.

Wei, J. J., Honda, H, 2003, *Effects of Fin Geometry on Boiling Heat Transfer From Silicon Chips with Micro-Pin-Fins Immersed in FC-72*, International Journal of Heat and Mass Transfer, 46, pp. 4059-4070.

Wei, B.Q, Vajtai, R., Jung, Y., Ward, J., Zhang, R., Ramanath, G., Ajayan, P. M., 2002, *Microfabrication Technology: Organized Assembly of Carbon Nanotubes*, Nature, 416, pp. 495-496.

Xiao, Z. L., Han, C. Y., Kwok, W. K., Wang, H. H., Welp, U., Wang, J., and Crabtree G. W., 2004, *Tuning the Architecture of Mesostructures by Electrodeposition*, Journal of the American Chemical. Society. 126, pp. 2316-2317.

Xu, J., Ji, X., Zhang, W., Liu, G., 2008, *Pool boiling heat transfer of ultra-light copper foam with open cells*, International Journal of Multiphase Flow, 34, pp. 1008–1022.

Yaddanapudi, N., Kim, J., 2001, *Single Bubble Heat Transfer in Saturated Pool Boiling of FC-72*, Multiphase Science and Technology, 12, pp. 47-63.

Yang, C-Y., Liu, C-F., 2008, *Pool Boiling Heat Transfer On Vertical Micro Porous Coated Surface In Confined Space*, Proceedings of the Sixth International ASME Conference on Nanochannels, Microchannels and Minichannels, Darmstadt, Germany.

Yuan, M., Wei, J., Xue, F., Fang, J., 2009, *Subcooled flow boiling heat transfer of FC-72 from silicon chips fabricated with micro-pin-fins*, Internaltional Journal of Thermal Sciences, 48, pp. 1416-1422.

Appendices I - VI

I. Richard Furberg, Shanghua Li, Björn Palm, Muhammet Toprak, Mamoun Muhammed, 2006, *Dendritically Ordered Nano-Particles in a Micro-Porous Structure for Enhanced Boiling*, Proceedings of IHTC-13 conference, Sydney, AU.

II. Shanghua Li, Richard Furberg, Muhammet Toprak, Björn Palm, Mamoun Muhammed, 2008, *Nature-inspired Boiling Enhancement by Novel Nanostructured Macro-porous Surface*, Advanced Functional Material, Vol. 18, pp. 2215–2220.

III. Richard Furberg and Björn Palm, 2011, *Boiling Heat Transfer on a Dendritic and Microporous Surface in R134a and FC-72*, Applied Thermal Engineering, 31, pp. 3595-3603.

IV. Richard Furberg, Björn Palm, Shanghua Li, Muhammet Toprak, Mamoun Muhammed, 2009, *The Use of a Novel Nano- And Micro-Porous Structure For Enhanced Boiling In a Plate Heat Exchanger*, Journal of Heat Transfer (special edition on porous media heat transfer), Vol. 131 (10).

V. Richard Furberg, Rahmatollah Khodabandeh, Björn Palm, Shanghua Li, Muhammet Toprak, Mamoun Muhammed, 2008, *Experimental Investigation of an Evaporator Enhanced With a Micro-Porous Structure in a Two-Phase Thermosyphon Loop*, Proceedings of 2008 ASME Summer Heat Transfer Conference, HT2008, August 10-14, Jacksonville, Florida USA.

VI. Rahmatollah Khodabandeh, Richard Furberg, 2010, *Heat Transfer, Flow Regime and Instability of a Nano- and Micro-Porous Structure Evaporator in a Two-Phase Thermosyphon Loop*, International Journal of Thermal Sciences, pp. 1183 – 1192.